Received: 16 August 2018 | Revised: 17 October 2018 | Accepted: 9 November 2018

DOI: 10.1002/er.4326

REVIEW PAPER

WILEY INTERNATIONAL JOURNAL OF ENERGY RESEARCH

Heteroatom-doped graphene and its application as a counter electrode in dye-sensitized solar cells

Nonjabulo P.D. Ngidi | Moses A. Ollengo | Vincent O. Nyamori

School of Chemistry and Physics, University of KwaZulu-Natal, Durban 4000, South Africa

Correspondence
Vincent O. Nyamori, School of Chemistry and Physics, University of KwaZulu-Natal, Westville Campus, Private Bag X54001, Durban 4000, South Africa.
Email: nyamori@ukzn.ac.za

Funding information
University of KwaZulu-Natal (UKZN); UKZN Nanotechnology Platform; National Research Foundation, Grant/Award Numbers: 103979 and 101357

Summary

The most frequently used counter electrode (CE) in dye-sensitized solar cells (DSSCs) is platinum on fluorine-doped tin oxide glass. This electrode has excellent electrical conductivity, chemical stability, and high electrocatalytic affinity for the reduction of triiodide. However, the high cost of metallic platinum and the poor electrochemical stability pose a major drawback in the commercial production. This has necessitated a search for a non-precious metal and metal-free electrocatalyst that demonstrates better catalytic activity and longer electrochemical stability for practical use in DSSCs. Graphene has been at the centre of attention due to its excellent optoelectronic properties. However, a defect-free graphene sheet is not suitable as a CE in DSSCs, because of its neutral polarity which often restricts efficient charge transfer at the graphene/liquid interface, irrespective of the high in-plane charge mobility. Hence, heteroatom-doped graphene-based CEs are being developed with the aim to balance electrical conductivity for efficient charge transfer and charge polarization for enhanced reduction activity of redox couples simultaneously. The elements commonly used in chemical doping of graphene are nitrogen, oxygen, boron, sulfur, and phosphorus. Halogens have also recently shown great promise. It has been demonstrated that edge-selective heteroatom-doping of graphene imparts both efficient in-plane charge transfers and polarity, thereby enhancing electrocatalytic activity. Thus, heteroatom-doped graphene serves as a good material to replace conventional electrodes and enhance power conversion efficiency in DSSCs. The focus is to reduce the cost of DSSCs. This review explores the performance of DSSCs, factors that influence the power conversion efficiency, and various physicochemical properties of graphene. It further outlines current progress on the synthetic approaches for chemical doping (substitutional and surface transfer doping) of graphene and graphene oxide with different heteroatoms in order to fine-tune the electronic properties. The use of heteroatom-doped graphene as a CE in DSSCs and how it improves the photovoltaic performance of cells is discussed.

KEYWORDS

counter electrode, dye-sensitized solar cells, graphene, heteroatom doped, renewable energytransparent conducting electrode

1 | INTRODUCTION

The United Nations sustainable development goal, number 7, advocates for clean and affordable energy for all. To attain this goal, the global focus has been on renewable energy sources. Sustainable renewable energy sources include solar,[1] geothermal,[2,3] biomass,[4] wind,[1] biofuels,[5] ocean waves, and hydroelectricity.[6,7] Solar energy has proven to be highly sustainable posing negligible release pollutants if any, thus having, minimal or zero negative impact on the environment.

2 | SOLAR CELLS

Solar cells are widely used for terrestrial applications and are economically competitive as alternative energy sources for domestic appliances, such as refrigerators.[8,9] Further, solar cells are used in various devices from handheld calculators to rooftop solar panels.[10,11] Solar cells are grouped based on the nature of materials used and the conversion efficiency.[12] Table 1 compares the efficiencies of various solar cells with first generation solar cells.

In the quest of addressing the challenges faced by current solar cells newer efficient solar cells are under intensive investigation. These include concentrated solar cells, polymer-based solar cells, nanocrystal-based solar cells (quantum dot solar cells), and dye-sensitized solar cells (DSSCs). These novel technologies, although promising, are yet to be commercially proven. The most favourable technology is the use of DSSCs as an alternative to silicon-based solar cells,[12] firstly, because they can function at low light intensities and are environmentally friendly, secondly, have simple fabrication process, low production cost, high efficiency, and feasibility to be printed on a flexible substrate. DSSCs differ from conventional semiconductor devices in that they separate the function of light absorption from charge carrier transport. They absorb the incident sunlight and exploit the capability of light energy to induce a vectorial electron transfer reaction.

TABLE 1 Energy conversion efficiency of different types of solar cells

Types of Solar Cells	Efficiency/%	Ref.
Single/monocrystalline Si	20.6	13
Polycrystalline Si	~12-14	12
Amorphous Si	10.1	14
Cadmium telluride (CdTe) thin film	13	15,16
Copper indium gallium selenide (CIGS) thin film	21.9	17
Nanocrystal	7.2	18
Polymer	3-9 and 10.8	19-21
Concentrated	~40	22
Organic	9.5	23
Dye-sensitized	7.8	24,25

The novelty of these solar cells emerges from the photosensitization of nano fine-grained titanium oxide (TiO_2) coated with active dyes, consequently improving the efficiencies of the cells.[26] Dye-sensitized solar cells enjoy the flexibility of expanding the range of applications where conventional solar cells are unsuitable. However, DSSCs suffer from a number of challenges, such as photodegradation of the dye molecule.[27] The dye photodegradation generally occurs when the dye is exposed to infrared and ultraviolet radiation leading to a shorter lifetime and poor stability of the DSSCs. The major cause is poor optical absorption of the dye-sensitizer, and the resultant effect is a lower conversion efficiency.

Dye-sensitized solar cells are made up of four components, namely, a dye sensitizer, a semiconductor electrode (photoanode), the electrolyte, and a counter electrode (CE) (Figure 1). The photoanode contains a mesoporous oxide layer (generally, TiO_2) which is deposited on a transparent conductive glass substrate.[28] The dye-sensitizer is covalently bonded to the TiO_2 layer to harvest light and produce photo-excited electrons. The performance of DSSCs is mostly dependent on the molecular structure of the dye-sensitizer. Three different classes of dye sensitizers have been reported to be used in DSSCs, such as metal-free organic sensitizers, complex sensitizers, and natural sensitizers.[29] The electrolyte is made up of a redox couple (generally, iodide/triiodide (I^-/I_3^-) and Co(2,2-bipyridine)$_3^{2+/3+}$)[30] in an organic solvent in order to accumulate electrons and cause dye-regeneration. The electrolyte also functions as a charge transport medium for the transmission of positive charge to the CE.[31] The electrolyte is expected to have low viscosity for faster electron diffusion to occur, high electrical conductivity, excellent contact between the CE and the nanocrystalline semiconductor, lack of absorption of light in the visible region, and no degradation of dye. The CE consists of a conductive glass substrate which is coated with platinum. It is mostly used to transport the electrons which come from the external circuit and go back to the electrolyte.[32,33] Accordingly, for effective charge transfer, the CE is required to display a high electrical conductivity and catalytic activity. Therefore, the catalyst must increase the rate of the reduction reaction.

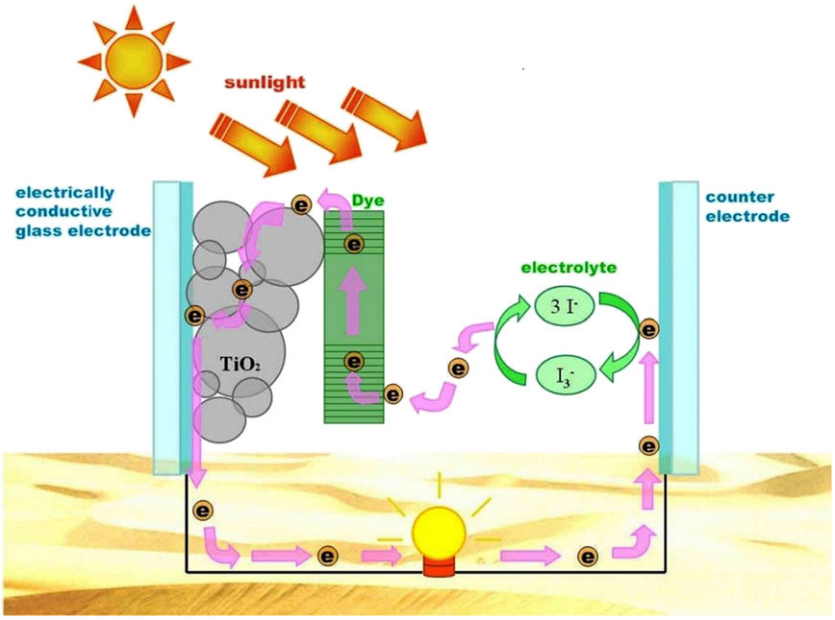

FIGURE 1 A schematic diagram of a DSSC[34] [Colour figure can be viewed at wileyonlinelibrary.com]

3 | MECHANISTIC ISSUES IN DSSCS

In DSSCs, the optical excitation of the dye causes electron promotion into the conduction band of the metal oxide. The promoted electrons are transported to the external circuit through the metal oxide film. A redox electrolyte is traditionally inserted into the film pores, which serves as a hole transporting material, and also serves to re-reduce the photo-oxidized dye and transfer the resultant positive charge to the counter-electrode[35,36] The net effect of the structural design is an optimized electronic coupling that is sufficiently large for charge separation to compete effectively with excited state decay, and small enough to minimize charge recombination. An optimum DSSC performance is attained when the recombination dynamics are as slow as possible but allows fast electron injection to compete effectively with excited state decay, thus, minimizing kinetic redundancy in the system. Another approach to minimize system kinetic redundancy is the addition of a secondary electron donor or acceptor species; this increases the spatial separation of the electron and hole and slows charge recombination without necessarily retarding charge separation. The physical separation of the injected electrons and the oxidized dye retards the recombination reactions and modulates surface dipoles and pacifies surface states. The reduced recombination losses improve photovoltaic device performance.[35]

Considering the solid-liquid interface at the CE, the interfacial charge-transfer mechanism requires an efficient electron transfer that is attributed to the strong overlap of wave functions between the excited states. In this case, an electron transfers adiabatically by occupying the bridging state in the lowest excited-state once the exciton diffuses to the interface region.[37] Thus, to induce the charge separation process, the closely lying single-particle states just above (energetically) this electron-transferring bridge state facilitate the exciton dissociation (complete transfer) to form the bound ion pairs. However, large vibronic couplings are expected among them because of the near degeneracy of these single-particle states and significant spatial overlap with the bridge state.[37] The near-degenerate single particle states enable efficient exciton dissociation and reduce the probability of the electron to recombine with the hole through the bridge state. Another possible mechanism for exciton dissociation is the single-phase rearrangement of the near-degenerate single-particle states as a result of geometrical distortions. The geometrical distortions induce strong coupling of electronic structure and, particularly, the t_{1u} state is split into a combination of singly and doubly degenerate states.[38] It should be noted that a covalent activation of the graphene surface, for instance, can change the relevant energetics by inducing a splitting of the degenerate lowest unoccupied molecular orbital (LUMO) states. Further, the energy alignment of electronic single-particle states at the interface is significantly altered in the excited state because of the transferring charge at the nanoscale heterojunction.

It has been recently suggested that a near degeneracy enables an asymmetric exciplex state that acts as an effective intermediate state for transferring charge thereby facilitating exciton dissociation. It can, therefore, be expected that the disruption of degenerate LUMO states in general accounts for a less efficient exciton

dissociation. Thus, covalent functionalization of graphene induces disruption of the LUMO degeneracy.[37] It can be argued that a larger wave function overlap in the excited state partly satisfies this important criterion and allows for a fast adiabatic electron transfer. However, the existence of such an adiabatic transfer channel alone may not solely lead to an efficient charge separation process unless there exists in the energetic vicinity other states that can facilitate the exciton dissociation efficiently. By functionalization of molecular chemistry at the surface, one can tailor the electronic structure such that the bridging state for the transferring electron forms near the conduction band minimum.[37] A conventional nonadiabatic electron-transfer mechanism can also serve to explain the observed ultrafast charge transfer assuming the semi-infinite acceptor states are in the conduction band of the metal oxide, and that the photoexcited electron within the dye has a very high total transition probability to the metal oxide.[35]

A judious asymmetric activation of the graphene surface with different chemical moieties can lead to a guided self-assembly of heteroatom doped-graphene sheets into hierarchically structured materials. The graphene edge and/or basal plane chemical activation may be *via* covalent or noncovalent interaction. These impart solubility, film forming capability, and enhanced chemical reactivity that modulate the properties for multifunctional applications.[39,40] For instance, Ju et al[41] recently reported edge-selective doping as a way of preserving the pristine graphene basal plane and further showed that edge-selenated graphene nanoplatelets are robust metal-free catalysts for the iodine redox reaction in the CE of DSSCs. The value of the charge transfer resistance, R_{ct}, at the CE-electrolyte interface indicates the effectiveness of the CE in regenerating the iodine species in the electrolyte. A lower R_{ct} value shows an enhanced reduction of triiodide ions on the CE-electrolyte interface, thereby increasing the availability of I^- ions on the dye-electrolyte interface. The resultant effect is the suppression of charge recombination in the photoanode and an increase in the open circuit voltage of the DSSCs. The iodine reduction reaction occurring at the CE/electrolyte interface is the major rate-determining step in DSSCs[42] and the energy of the I atom can serve as a good descriptor for the iodine reduction reaction.

4 | COUNTER ELECTRODES IN DSSCS

The CE plays a big role in DSSC. It is responsible for catalysing the reduction of I_2 to I^- after electron injection.[43] The CE is expected to be highly conductive and highly catalytic. Different methods have been reported for the preparation of CEs, such as chemical vapour deposition,[44,45] chemical reduction,[46,47] hydrothermal reaction,[46,48] electrochemical deposition,[49,50] thermal decomposition,[51,52] in situ polymerization,[53,54] and sputter deposition.[55-57] The preparation approach influences the morphology, surface area, particle size, electrochemical, and catalytic properties of the electrode.[58] The large surface area and small particle size generate more catalytically active sites and enhance the improvement of the electrocatalytic activity of CE.[58] The preparation methods of CEs are different based on the material from which they are made.

Different CEs have been employed such as conductive substrates (conductive glass substrate, conductive polymer substrate and metal substrate),[59] transparent CEs,[60,61] flexible CEs,[62] polymer CEs,[63,64] transition metal compound CEs (carbides and nitrides, chalcogenides, oxides),[65] hybrid CEs (platinum-loaded hybrids, transition metal compounds (TMCs)/carbon hydride, carbon/polymer hybrids, polymer/TMC hybrids),[66] metal and alloy CEs (platinum CE),[67] and carbon CEs (carbon black nanoparticles, carbon nanofibers, carbon nanotubes, graphene).[68]

In most cases, platinum-loaded conducting glass has been used as the CE because of its good conductivity and high catalytic activity.[69] However, when the platinum-loaded conducting glass is working against I^-/I_3^- in the electrolyte, it possesses a high corrosion stability.[69,70] Consequently, different platinum-based CEs have been intensively used, such as, platinum nanoparticles and platinum composite materials.[71-73] Platinum nanoparticles are the best transparent and stable CEs because of their high density of catalytic sites and high surface area.[71] Platinum nanoparticles have been employed in DSSCs to produce a power efficiency of 9.75% whilst a planar platinum produced an efficiency of 7.87%. Similar studies have been conducted to exhibit the photovoltaic and catalytic behaviour of various platinum facets.

Zhang et al[74] demonstrated that different Pt facets, eg, Pt(100), Pt(111), and Pt(411), exhibit different photovoltaic performance. Pt (111) was found to have a lower charge transfer resistance than other facets. The electrocatalytic activity was also improved by using a platinum composite containing a polymer and carbon. Yen et al[72] reported the use of a Pt composite composed of Pt nanoparticles supported on fluorine-doped tin oxide (FTO) and platinum nanoparticle/graphene composite (Pt NP/GR) in DSSCs. Its photovoltaic performance and physical properties were compared with those of Pt films and graphene. It was revealed that Pt NP/GR have a higher surface area, hydrophilicity, and electron transfer rate because of the presence of oxygen in graphene. Pt NP/GR showed a

photovoltaic performance of 6.35%, which was much higher than that of graphene and Pt film as a CE.[72]

The problem with using platinum-based CEs is that Pt is very expensive due to its wider range of applications (especially in the vehicle industry).[75] Therefore, platinum-free materials are employed in DSSCs as a replacement for platinum-based materials. Various materials, such as carbides,[76] nitrides,[77] transition metal sulfides,[78] and carbon,[79] are employed as CEs. The use of carbon materials in DSSCs is quite appealing because they are cheap, commonly available in large quantities, exhibits excellent catalytic activity, is environmental friendly, and is corrosion resistant.[43]

However, the photovoltaic performance of carbon in DSSCs has been reported to be poor compared with that of platinum-based materials.[80] Energy conversion efficiencies of 3.9%, 4.5%, and 5.75% in DSSCs has been obtained when carbon nanotubes,[81] activated carbon,[43] and graphite,[82] respectively, are used as CEs. The disadvantage of using carbon-based CEs is that they require a large amount of carbon to produce a comparable efficiency to platinum-based CEs.[83] This makes the device opaquer and bulkier. However, different modifications of carbon have been performed in order to enhance the photovoltaic performance.[83]

Carbon is an extremely light and versatile material. The two common forms of carbon, diamond, and graphite (Figure 2A,B). Diamond is hard and transparent whereas graphite is very soft and opaque. They differ in the structure or the hybridization of the carbon atoms, for example, graphite is sp^2-hybridized while the hybridization in diamond is sp^3. Graphite is a good thermal and electric conductor within the layers; however, it is a poor thermal and electrical conductor between the layers. Due to its electrical conductivity, graphite is employed as an electro-chemical electrode.[85] Graphene is considered as the fewest layer of graphite[86] (one atom thick sheets). Graphene and its derivatives have been applied in solar cells since 2004.[87] Graphene has been recommended as a substitute material for the CE. This is because it possesses a large surface area, excellent electrocatalytic properties, and high optical transmittance. It is frequently chemically doped with different heteroatoms to optimize its structure and tune its conductivity and catalytic activity with the aim of further improving the power conversion efficiency in solar cells.[72,88] The current work offers an in-depth review of chemical doping of graphene, explores the creation of a band gap in graphene, and revisits heteroatom-doping of graphene and its effect on electrical conductivity. It further demonstrates the potential of heteroatom-doped graphene as a CE for DSSCs.

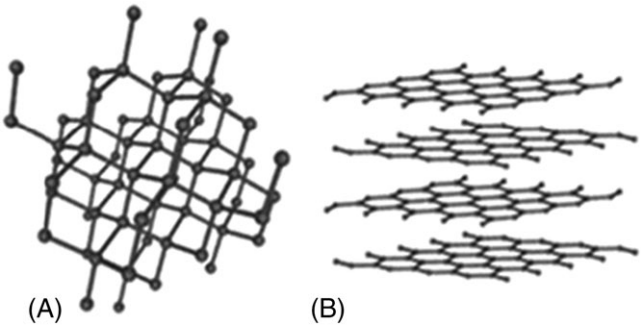

FIGURE 2 The common allotropes of carbon: A, diamond and B, graphite[84]

5 | GRAPHENE AS A COUNTER ELECTRODE MATERIAL

Graphene is a single, thin layer of carbon, a latest member of carbon-based nanomaterials. It is the fundamental structural component of other allotropes, such as diamond, fullerenes, and carbon nanotubes.[89] In graphene, the carbon atoms are bonded together in a hexagonal honeycomb lattice. It is a two-dimensional nanostructured carbon-based material.[90] The name graphene was introduced in 1994 by Boehm, Setton, and Stump.[91]

The lateral dimensions of graphene may vary from several nanometres to microscale, eg, monolayer, bilayer, and tri-layer.[92] Monolayer graphene is also called single-layer graphene and is preferred for use in high-frequency electronic applications.[92] It possesses a high mobility, high optical transparency, and high surface area.[92] These properties allow monolayer graphene to be a good material for improving the efficiency in DSSCs.[92,93] Bilayer or tri-layer graphene consists of two or three layers, respectively. As the number of layers increases, they display different electrical properties.[87] Monolayer graphene has a zero-band gap while bilayer graphene has a parabolic band structure (effective mass $m = 6.6 \times 10^{-38}$ kg),[94] and its band gap can be varied by using an external perpendicular electrical field.[89,95,96] Similarly, tri-layer graphene also has a parabolic band; however, the effective mass ($m = 9.3 \times 10^{-38}$ kg) is larger than that of bilayer graphene.[94]

There are different types of graphene-based nanostructures with various morphologies that have been reported. These are zero-dimension graphene quantum dots (GQDs), one- dimension graphene nanoribbons (GNRs), and two-dimension graphene nanosheets (GNSs).[97] GQDs have nanometre-scaled graphene particles that contains a sp^2-sp^2 carbon bond.[98] They have a high surface area and high transparency which allows them to be applied in energy and display applications. GNSs are metal-like conductors with zero-bandgap while GNRs can be either semiconducting or metallic.[99] These

new graphene materials have unique electrochemical properties in comparison with pristine graphene. The properties of GNRs and GQDs can be tailored by modulation of the respective edges and sizes.[100] For example, GNRs having a width that is narrower than 10 nm have good semiconducting characteristics while GNRs that have a width larger than 10 nm have weak semiconducting characteristics.[97] The mainly zigzag-edged GNRs (2.3 nm wide) show a smaller bandgap of 0.14 eV, while the armchair GNRs (2.9 nm wide) have a bandgap of 0.38 eV, which indicates that the higher concentration of zigzag edges causes the energy gap to decrease because of the staggered sub-lattice potential through the zigzag terminated edges.[101,102]

Normally, the carbon atom contains a total of six electrons; two electrons are situated in the inner shell while the other four electrons are in the outermost shell and are available for chemical bonding. However, the carbon atom in graphene is bonded to three other atoms because of sp^2-hybridization. The other electron in the dimension remains unbonded so that it can be used during electronic conduction.[103] In a molecular orbital perspective, the stability of graphene is caused by the tightly packed carbon atom and sp^2 orbital hybridization with p_x, p_y, and s as atomic bonding orbitals on each constrained carbon atom creating three strong σ bonds along with three other surroundings atoms.[104,105] Each neighbouring atom has an overlapping p_z orbital which forms a valence band (filled band of π orbitals) and the conduction band (empty band π^* orbital). These bands are the essence of the electron properties of graphene by a means of a half-filled band which allows free-moving electrons.[106] Figure 3 shows the band structures of graphene and the zoomed energy bands of the Dirac point (showing the junction of the conduction band and valence band at the K and K′ points in the reciprocal space).

Graphene possesses high electrical conductivity, and zero-gap as illustrated in Figure 3. Thus, it functions as a semimetal. This is because its conduction band can make contact with the valence band at the Dirac point.[107] Consequently, a device which is fabricated from zero-bandgap graphene tends to lose the advantage of the low static power consumption and is difficult to switch off due the to the very low on/off ratio. Hence, creating a well-tuned and sizeable bandgap is a great challenge in graphene-based electron devices.

The absence of a bandgap is ascribed to the similar environment of the two sublattices of the carbon atoms in the unit cell of the graphene.[107] The Fermi level in an unperturbed graphene sheet coincides with the Dirac point where minimum conductivity occurs.[108] Figure 3B shows pristine graphene exhibiting a strong ambipolar field effect which further demonstrates the possibilities of doping. N- and p-type graphene (Figure 3C,D) occurs when there is a shift in the Dirac point in relation to the Fermi level caused by chemical modification.[109]

Many techniques have been proposed to create a band gap in graphene; among them are bilayer graphene with an induced band gap (GNRs and GQDs) or a substrate-induced band gap. The chemical functionalization of graphene causes modifications of the carbon sp^2 lattice.[110] This changes the surface, chemical, and electronic properties of graphene and helps in enhancing free charge-carrier densities and electrical conductivity.[110]

Chemical modification can be achieved by covalent and non-covalent interactions[109] for instance, atom doping of graphene,[111,112] a phenomenon made possible by functionalizing graphene, making use of the unsaturated structure of graphene. Non-covalent modification makes use of hydrogen bonding,[113,114] coordination bonds,[115,116] electrostatic interactions,[117,118] π-π stacking interactions,[119,120] and van der Waals forces.[121-123] The interactions that occur through non-covalent bonding are relatively weak compared with those from covalent modification.[109] Covalent modification of graphene forms stronger bonds between the modifier and graphene. The

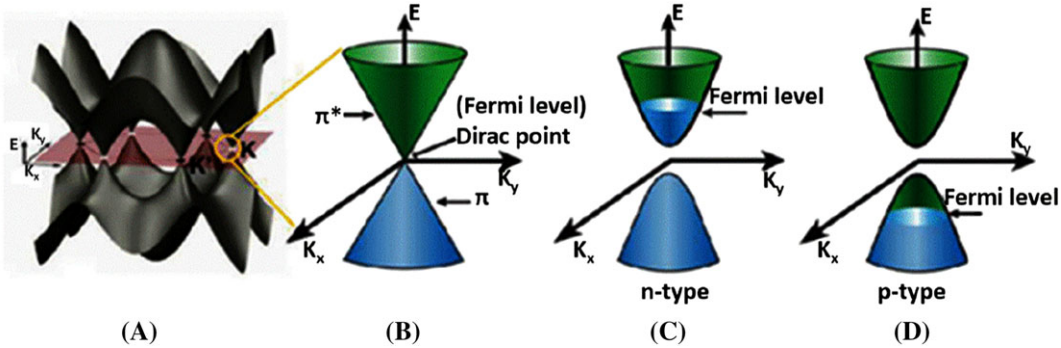

FIGURE 3 (A) The 3D band structure of graphene[104]; (B) the lower energy band structure of graphene with the two cones which intersect at the Dirac point and the bandgap of the energy band structure of (C) n-type graphene and (D) p-type graphene[105] [Colour figure can be viewed at wileyonlinelibrary.com]

problem with covalent modification is that the bonds are unrecognizable because they lack functional groups that can be conjugated with carbon in graphene.[124]

Chemical modification, such as hydrogenation,[125] oxidation of graphene,[126] chemical doping (heteroatom-doped graphene),[127,128] reduction of graphene oxide (GO),[129,130] and fluorination,[131] is an alternative way to create a band gap in graphene. Balog et al[132] investigated the bandgap opening process onto the Moire superlattice locality of graphene by using mosaic adsorption of atomic hydrogen. In this approach, graphene that had been synthesized on an Ir(111) substrate was exposed to atomic hydrogen. This resulted in partially or fully hydrogenated graphene which displayed different thermopower, magneto-electronic, and structural properties. Consequently, several working groups have reported the chemical doping (heteroatom doping) of graphene as a means to improve the performance of graphene-based devices, thus opening up a wider range for the application of graphene.[88,133,134]

This review focusses on heteroatom-doped graphene as a suitable material for the construction of CEs in DSSCs. In particular, the following aspects are discussed:

- The potential of heteroatom-doped graphene as a CE for DSSCs.
- The ability of chemical doping of graphene to create an energy bandgap and form catalytic sites.
- The enhanced electrical conductivity of heteroatom-doped graphene.
- The dependency of the heteroatom-doping level on the dopant and the different doping techniques.
- The synergistic effect between the co-dopants and graphene to provide well-defined properties.

Hence, the review should offer in-depth comments on chemical doping of graphene, explore the creation of a band gap in graphene, revisit heteroatom-doping of graphene and its effect on electrical conductivity, and demonstrate the potential of heteroatom-doped graphene as a CE for DSSCs.

6 | HETEROATOM-DOPED GRAPHENE

Chemical doping not only creates the bandgap but also controls the concentration and type of charge being injected into graphene.[72,135,136] It aids in modifying the electronic properties of graphene.[72] There are two types of chemical doping of graphene, namely, surface-transfer doping and substitutional doping. Surface-transfer doping occurs when a functional group is added on the graphene sheet.[137] It is attained by electron exchange between a semiconductor and a dopant that accumulates the electrons on the surface of a semiconductor. Thus, it is also called adsorbate-induced doping. During surface transfer doping, the structure of graphene is not disrupted.[138,139] Therefore, this doping process is reversible.[140] The charge transfer depends on the density of states of the dopant in the Fermi level of graphene.[141] The dopant acts as a donor when the charge transfer is found above the Fermi level of graphene, whereas when it is below the Fermi level, the dopant acts as an acceptor.[138]

Substitutional doping is attained through the replacement of a carbon atom in the graphene lattice by another atom which has a different number of valence electrons.[72,142] Introduction of heteroatoms gives graphene more active sites.[72,143] Deng et al[76] reported that the addition of a heteroatom with a different electronegativity from carbon reduces the electroneutrality of graphene and forms an active site. The active site causes graphene to exhibit unique physicochemical properties[76] characteristic of the nature of the heteroatom in question. The heteroatom can be an electron acceptor or electron donor. Substitution with an atom with more valence electrons than carbon brings about n-type conductivity, whereas an atom with fewer valence electrons results in p-type conductivity[144] as described earlier. The synthetic methods for producing substitutional doped graphene are classified into two categories: post-treatment and in situ approaches.

The in situ approaches can be achieved by using different methods, namely ball milling,[145,146] chemical vapour deposition (CVD)[146] and bottom-up synthesis.[147,148] Similarly, there are different types of post-treatment methods, such as thermal annealing,[119,133] wet chemical methods,[149,150] plasma treatment,[151] and arc discharge[152] approaches. Different kinds of dopants have been incorporated in graphene; these include oxygen, nitrogen, boron, sulfur, and phosphorus.[72] However, nitrogen and boron have caught the attention of most scientists. This is because they both have atomic radii which are similar to that of carbon. They also have a similar size, and hence, their incorporation into graphene is effortless.

6.1 | Morphology of heteroatom-doped graphene

The adsorbed heteroatoms on graphene through doping distort the carbon atoms vertically, with almost no modification of the in-plane structures. Generally, heteroatoms distort the local geometry of graphene by locally rehybridizing the bonding from $pz + sp^2$ to sp^3 which causes a gap to open. This spin is quenched by the

presence of a rotated C—C bond (a Stone-Wales defect) adjacent to or distant from the heteroatom.[153,154] The net effect is that the ground state shows a ferromagnetic order, with a total energy of a few tens meV lower than the nonmagnetic ground state. The heteroatom adsorption opens a gap that depends on the guest atom, and the optical conductivities indicate fine structures at the band edge. However, the spin-orbit coupling, and the nonzero off-diagonal components of the conductivity predict Kerr and Faraday effects without an external magnetic field[154] on doped graphene sheets. Graphene oxide (GO), which is an oxidized derivative of graphene, with an oxygen-rich surface, has an improved dispersion in aqueous mixed matrices. Co-doping of heteroatoms synergistically enhances the asymmetric spin and charge densities of carbon atoms that are responsible for superior electro-catalytic activity.[155] Co-doping of N and S atoms on graphene nanosheets substantially enhances the asymmetric spin density as well as the charge density, which are responsible for the electrocatalytic activities.

6.2 | Oxygen-doped graphene

Oxygen is one of the elements with higher electronegativity. It cannot be substitutionally doped into the graphene lattice because of its larger size and strong electronegativity. However, graphene can be covalently functionalized with a plethora of oxygen moieties.[156] These oxygen functionalities on the graphene sheet exhibit a surface-transfer doping effect. GO is widely studied, and it is oxidatively synthesized from graphite powder.[129] The introduction of oxygen functionalities in the graphite structure occurs during the oxidation of graphite with the use of a strong oxidizing agent.[156] This not only changes the structure but also expands the layer separation and causes the material to become hydrophilic. When graphite is exfoliated in water *via* sonication, a final product, usually consisting of a single or a few layers of graphene, called GO is realized. The GO and graphite oxide differ in the number of layers. Graphite oxide consists of a multilayer system while GO has a few layers or consists of monolayer flakes.[156]

This oxidation of graphite can be regarded as oxygen-doped graphene. The GO lattice contains hydroxyl (—OH) and epoxyl groups (—C—O—C) on the basal planes, while at the edges, it has carboxyl (—COOH) groups. The carbon atoms on which the oxygen groups are attached are transformed from the sp^2 to the sp^3 hybridization state with local distortions of the graphene planar structure. This disruption of the sp^2 hybridization state creates a bandgap in graphene and causes GO to be non-conductive.[157] It has been reported that GO consists of a heterogeneous electronic structure because of the assorted hybridizations (sp^2 and sp^3).[158]

Addition of oxygen to graphene can be performed by using either a top-down or a bottom-up wet chemical oxidation.[159] The top-down wet chemical oxidation method is widely used because it generates a high yield of GO.[160] It involves the oxidation of graphite *via* different chemical routes such as Brodie's oxidation method (fuming nitric acid and potassium chlorate),[161] Staudenmaier method (fuming HNO_3, concentrated H_2SO_4, and $KClO_4$),[162] Hofmann method (concentrated HNO_3, concentrated H_2SO_4, and $KClO_4$),[163] and Hummers method (concentrated H_2SO_4 in the presence of $KMnO_4$).[164] Hummers method has been reported to be the best and simplest method to yield good quality GO.[165-167]

Graphene oxide acts as an electrically insulating material because of the structural disorder applied by the C—O bonds (sp^3) which disrupts its conductive π-network.[168] The disruption in electrical conductivity can be restored by reduction of GO. The oxygen functional groups in GO can be removed by using different methods such as chemical treatment or thermal annealing to form reduced-GO (rGO). rGO can be synthesized by using different chemical techniques such as chemical reduction,[169-171] thermal reduction,[172] microwave and photoreduction,[173,174] photocatalyst reduction,[175] and solvothermal/hydrothermal reduction.[176-179] However, the most frequently used technique for reduction is chemical reduction. rGO has similar properties to those of GO. Mathkar et al[180] reported that reduction of GO also modifies the bandgap. The structural altering of GO to rGO causes gradual changes in thermal stability,[181] electrical conductivity,[182] carrier mobility,[183] and optical bandgap.[184]

The chemical reduction method uses different reducing agents, such as amino acid,[185] sodium borohydride,[130] urea,[186] hydrazine hydrate,[187] ascorbic acid,[188] strong alkaline solution,[189] and glucose,[190] and this may involve ultrasonication of the chemicals with GO in water.[191] Chemical reduction of GO produces rGO and large quantities of graphene.[192] The rGO formed after ultrasonication bears resemblance to graphene, yet it contains residual oxygen and structural defects. After the reduction process, some of the oxygen-containing groups are removed, and the π-electron conjugation is partially reinstated in the graphene aromatic system.

The main challenge of the chemical reduction method is the use of hazardous chemicals as reducing agents, eg, sodium borohydride, and thermal treatment consumes a lot of energy. Therefore, green reduction methods are now sought as alternative approaches, eg, the photothermal reduction method.[192] Photothermal reduction does not require the use of chemicals and high

temperature annealing. Cote et al[193] demonstrated that GO can be reduced by using a flash-reduction approach whereby GO is exposed to a pulsed Xe flash under ambient conditions. Recently, Chien et al[194] reported that the photoluminescence properties of rGO can be controlled by using a photothermal reduction method at different exposure times.

6.3 | Nitrogen-doped graphene

Nitrogen, with an electronic configuration of $1s^2 2s^2 2p^3$, is a natural choice as a dopant. In the periodic table, it is situated next to carbon ($1s^2 2s^2 2p^2$). It possesses one more valence electron than carbon. It has a higher electronegativity ($\chi = 3.04$) than carbon ($\chi = 2.55$).[195] Nitrogen atoms tend to donate electrons into graphene when incorporated into the basal plane of graphene occasioning n-type (negative) charge carrier characteristics. The n-type graphene occurs when a group 15 element is used as a dopant. Group 15 elements have five valence electrons and, thus, can donate an electron to the four-valent host material. Doping with nitrogen creates polarization in the sp^2 carbon network which influences the chemical and physical properties of graphene.[196] It had been reported that nitrogen doping can tune the characteristics of graphene materials, by creating a bandgap and inducing charge-carrier characteristics. The bandgap creation occurs near the Dirac point by suppressing the nearby density of states and granting graphene semiconducting properties.[105] Zhang et al[197] reported a bandgap of 0.16 eV which demonstrated that doping with nitrogen tunes the electrical properties of graphene. Shao et al[198] also demonstrated that the presence of nitrogen atoms in graphene improves their ability to donate electrons to the adjoining carbon atoms.

Nitrogen-doped graphene (N-doped graphene) usually has three common bonding configurations within the carbon lattice. These include graphitic-N (or quaternary-N), pyridinic-N, and pyrrolic-N atoms (Figure 4).[199] Pyrrolic- and pyridinic-N occur at the defects sites, and these defects impose the p-doping effect through withdrawing of electrons from the graphene sheet.[199] Pyridinic-N refers to a nitrogen bonded to two carbon atoms at the edges which donates one p-electron to the

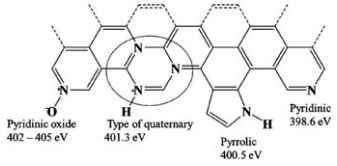

FIGURE 4 Schematic diagram of the bonding configurations of nitrogen atoms in N-doped graphene[199]

π system, while the pyrrolic-N refers to nitrogen atoms that donate two p-electrons to the π system.[200] In the graphitic-N, the nitrogen atom sits in-plane, replacing the carbon atoms in the hexagonal ring. These bonding configurations have different hybridization states of the nitrogen atom, which in turn has some effects on the electrical properties of N-doped graphene.[199] Quaternary-N and pyridinic-N are sp^2 hybridized since the nitrogen atom is coordinated to two atoms, while pyrrolic-N is sp^3 hybridized.[199] Beside these three-bonding configurations, nitrogen oxides of pyridinic-N have been discovered in both nitrogen-doped carbon nanotubes and N-doped graphene.[198,201] This configuration occurs when the nitrogen atom bonds with one oxygen and two carbon atoms. N-doped graphene and pristine graphene have different properties. For example, the charge distribution and spin density of carbon atoms in N-doped graphene will be affected by the neighbour nitrogen dopants.[76,202] This creates an "activation region" on the surface of graphene. This activation region can participate in catalytic reactions known as oxygen reduction reactions (ORR).

When monolayer graphene has been successfully doped with nitrogen, the Fermi level moves over the Dirac point,[203,204] and the density of states near the Fermi level is suppressed.[205] This results in band opening between the valence band and conduction band. This band gap enables N-doped graphene to be further applied in semiconducting devices.[205]

6.3.1 | Preparation of N-doped graphene

N-doped graphene can be synthesized in two different ways, either by post-synthesis treatment or by direct synthesis. The post-treatment method mostly results in surface doping only, while the direct synthesis method leads to homogeneous doping.[206] Specifically, post-synthesis treatment can be performed by using different techniques such as plasma treatment, hydrazine (N_2H_4) treatment and thermal treatment.[207] However, the direct synthesis involves solvothermal, arc discharge, and CVD.[208]

Post-synthesis treatment

The thermal treatment strategy is an extensively used approach to introduce nitrogen into graphene frameworks. This approach enables the use of various dopant precursors in the synthetic method (Table 2). Doping of graphene or GO with nitrogen-containing compounds is performed through high temperature and hydrothermal treatment. Compounds containing nitrogen such as urea, melamine, cyanamide, polyaniline, ammonia, and

TABLE 2 Synopsis of heteroatom-doped graphene doping approaches

Approaches	Advantages	Shortcomings	Ref.
CVD	•Easy to scale-up the reaction •Concurrently doping and growth of large sheet of graphene •Good reproducibility	•Sometimes, it can produce hazardous waste gases •Product may not be pure (due to hydrogen incorporation) •High process temperatures	169,209-211
Microwave-plasma CVD (MPCVD)	•Requires low temperature •Results in high level of doping	•Slow and two-step process •Expensive and more complex	212,213
Arc discharge	•Mass production	•Results in low doping level •Requires high voltage	152,214
Thermal annealing	•Easy to control doping level •Allows various choices of dopant precursors (solids, liquids and gases)	•Requires high temperature •Results in low doping level	215,216
Plasma treatment	•Short reaction time •Consume low power	•Produces low yield	217

hydrazine have been used as nitrogen sources.[179] It has been reported that when graphene is heated with ammonia at temperatures of 800°C or above N-doped graphene is obtained.[218,219] High temperature annealing of graphene has resulted in N-GNRs.[220]

Gou et al[218] reported that the yield of N-doped graphene synthesized from the thermal treatment is relatively low, specifically having a doping level of 1.1% at a temperature of 1100°C. However, Geng et al[219] discovered that at temperatures of 800°C and 900°C, there was highest nitrogen doping level of 2.8%. The low nitrogen content may be ascribed to high temperature which breaks the graphene C—N bonds lowering defect numbers in graphene.[219] They argued that nitrogen doping in graphene more likely happens at the edge and defect sites.[219] They also proposed that more dominant bonding configurations which occur during high temperatures are pyrrolic-N and pyridinic-N.[219] However, Wang et al[220] concluded that the nitrogen atom insertion in GNRs favours edge functionalization. All these reports showed that temperature has a crucial impact on increasing level of N-doped graphene.

Apart from graphene, GO has also been employed in the synthesis of N-doped graphene using thermal treatment with different nitrogen precursors.[221] Sheng et al[222] investigated the effect of high temperature between 700°C and 1000°C during the process of annealing GO with melamine. They reported that at these higher temperatures, the GO was not only doped with nitrogen but also the oxygen functional groups were reduced. The higher the temperature, the higher the reduction of oxygen functional groups. Similar findings were reported by Li et al[119] where they reported that the high temperature does not only reduce oxygen functional groups but also lowers the nitrogen content. However, Sliwak et al[223] reported the nitrogen-doped reduced GO obtained from hydrothermal route gave very high nitrogen content of 10.9% to 13.4%. Hence, no single conclusion can be drawn as results are contradictory.

N-doped graphene tends to have different layer distribution which is highly dependent on the synthesis parameters, especially temperature. Many researchers have reported that doping of GO at higher temperature results in few-layer N-doped graphene.[224-226] However, Ying et al[224] reported few-layer N-doped graphene synthesized at a lower temperature of 180°C. N-doped graphene is not only highly dependent on growth temperature but also on the synthetic mass ratio of nitrogen source and GO. The highest nitrogen doping (10.1%) is attained when a mass ratio of 0.2:1 of GO to melamine (nitrogen source) at a growth temperature of 700°C[222] is employed. Li et al[119] demonstrated that annealing GO at 500°C under NH_3 atmosphere can reduce GO and dope the graphene with 5% nitrogen content.

Direct synthesis

Arc discharge approach Arc discharge method has been employed to synthesize carbon-based materials such as carbon nanotubes.[227] It was shown that N-doped graphene synthesized from nanodiamond transformation have higher nitrogen content as compared with those synthesized from graphite.[228] In order to synthesize N-doped graphene, it requires buffer gases as nitrogen sources.[152] Li et al[152] reported N-doped multi-layered graphene sheet synthesized from arc discharge using

ammonia as a nitrogen precursor. They showed that the nitrogen content was approximately 1% which was consistent with what Rao et al[228] discovered. Rao et al[228] made use of ammonia and pyridine as nitrogen source, and the XPS data revealed that the samples had a nitrogen content of 1% and 0.6%, respectively. The arc discharge method is capable of synthesizing N-doped graphene in high purity and large quantities. However, the disadvantage of this method is that in the graphene structure, only a small quantity of nitrogen (Table 2) can be introduced.[228] By controlling parameters such as exposure time and plasma strength, the doping level could be optimized and regulated.

Chemical vapour deposition Chemical vapour deposition is a versatile technique used in the synthesis of carbon-based nanostructures like graphene. It can produce large defect-free and few or single-layered graphene films.[229] It is highly dependent on the three parameters namely, growth temperature, catalyst, and a precursor. CVD method works by decomposing hydrocarbon gases under high temperature with the aid of a catalyst to form sp^2 carbon species. The catalytic growth mechanism makes the CVD method a suitable way to dope graphene films with different heteroatoms, especially to directly incorporate heteroatoms into the carbon lattices.[230] The doping occurs by reacting liquid, solid, or gaseous precursors that have desired foreign atom along with graphite in the growth furnace. The CVD method is preferable because it is easy to scale-up the catalysing process (Table 2), is independent of substrate size, and is known to produce high quality N-doped graphene.[208]

The N-doped graphene in the CVD can be synthesized using hydrocarbon gases[231] with metal single crystals (Ru, Co, Ni, and Cu foils)[232] at high temperature.[205] Ni and Cu foils are most frequently used metal single crystals because of their unique solid solubility of carbon. Ni foil possesses a considerable solid solubility, while Cu foil possesses a very limited solubility of carbon; therefore, the carbon cannot diffuse to a great depth in the Cu substrate. However, Cu substrates are advantageous because of their graphene growth which is self-limiting, meaning the graphene growth stops after one layer is formed.

Different precursors are used in the process of doping graphene such as liquid, solid, and gaseous precursors. Nitrogen-containing functional groups could be doped in graphene by reacting graphene with nitrogen-containing reagents (urea, NH_3, and nitric acid) or through carbonizing/activating of nitrogen-rich carbon precursors, such as pentachloropyridine, polypyrrole, and pyrimidine. Other nitrogen-containing liquid precursors, such as acetonitrile and pyridine have also been used for the synthesis of N-doped graphene.[233,234] Some recent work has been based on gaseous nitrogen precursors such as ammonia.[205] Normally, the gaseous precursor works in conjunction with the other precursor (multi-precursor), while the liquid and solid precursors can function as a single precursor.[235] It should be noted that multi-precursors require multiple processes whereas the single precursors are more convenient and easier to control.

The problems with gaseous precursors are that they are hard to handle and transport and thus expensive, compared with liquid/solid ones. Consequently, liquid precursors are more attractive for doped graphene growth.[233,234] The N-doped graphene is formed on the surface of the catalyst when the precursors separate and recombine through precipitation. This favours large-area and high-quality N-doped graphene when liquid precursors are employed.[236] The layer distribution of N-doped graphene varies in different studies depending on the type of nitrogen source used. The liquid precursors such as pyridine[234] and acetonitrile[233] are reported to produce monolayer N-doped graphene. Interestingly, N-doped graphene formed from gaseous nitrogen precursor (or gas mixtures), C_2H_4/NH_3,[237] are monolayer, while a gas mixture of CH_4/NH_3[238] produces few-layer nitrogen doped graphene.

The formation of N-doped graphene depends on skeletal bonds of the liquid precursors,[239] eg, acrylonitrile contains a C—C single bond, C═C double bond, and C≡N triple bond. However, it cannot easily dope graphene. Pyridine contains C—C single and C═C double, and C—N single and C═N double bonds. It is only C═C double bonds that have been shown to easily form N-doped graphene. This is because C—C bonds are easy to break at lower and higher temperatures while the C═C bond and C≡N bond are left at the surface of the catalyst. The C≡N bond is removed from the surface of the catalyst using high temperatures above 400°C resulting in volatile molecules, whereas, skeletal bonds in pyridine contain lower bond energies that cause an increase in the formation of N-doped graphene.[236]

The doping level in CVD method can be controlled by altering the flow rate and ratio of both carbon and nitrogen.[240] Wei et al[205] reported that nitrogen decreases from 8.9% to 3.2% or 1.2% when NH_3/CH_4 ratio was reduced from 1:1 to 1:2 or 1:4, respectively. Further, the nitrogen bonding configuration in N-doped graphene differs with various studies. When Cu is used as a catalyst with a precursor of CH_4/NH_3 in a ratio of 1:1, then it results in quaternary N.[205] But when a catalyst Cu was used with CH_4/NH_3 (5:1) as a precursor, the N-doped graphene obtained mostly comprised pyridinic-N.[238] Pyridinic-N is dominant when a different precursor (C_2H_4/NH_3) is used

with Cu as a catalyst.[240] Zhang et al[241] reported a low-cost synthesis of high quality N-doped graphene with nitrogen content of 3.72% (Table 3) and demonstrated that the bonding was primarily pyrrolic-N configuration. This N-doped graphene was synthesized from urea as N source and methane as carbon source, on the Cu substrate using CVD.

Pyrolysis of GO and melamine in an argon atmosphere at 1050°C has been reported to have a nitrogen content of 2.48%.[242] The decrease in temperature causes an increase in doping concentration. Lu et al[208] reported that if the growth temperature in CVD is reduced, the atomic (nitrogen) percentage is raised from 2.1% to 5.6% when 1,3,5-triazine on Cu metal substrate are used (Table 3). Notably, researches have revealed that nitrogen doping is highly dependent on the growth temperature and flow rate when the CVD method is employed.[239,243]

6.4 | Boron-doped graphene

Boron is also an adjacent element to carbon in the periodic table and is suitable for doping. It can be chemically doped in the graphene lattice, just like nitrogen. Boron has one fewer valence electron than carbon. Three valence electrons participate in graphene doping bond formation with resultant single electron deficiency. This electron deficient nature induces a p-doping effect and a downshift towards the Dirac point in the Fermi level. It has been forecast that the Fermi level is highly dependent on the doping level.[244] It decreases to approximately 0.65 eV when the doping level of boron is 2% and goes even higher when there is a higher doping level.[228] Boron doping induces a p-type (positive) graphene. However, this doping may trigger chemical and electrochemical activity in the basal plane of graphene.

Boron-doped graphene (B-doped graphene) has two different bonding configurations, ie, either graphitic-boron (BC_3) or boron silane (BC_4).[245] BC_3 configuration is obtained due to replacement of carbon by boron in the hexagonal carbon lattice, whereas the BC_4 configuration is acquired because of the edge site defects.[245] In-plane BC_3 (in-plane substitutional doping) has been reported to be more stable than out-of-plane doping.[246] The charge polarization occurs among electron-deficient boron atom and neighbouring carbon atom. During doping, it retains the sp^2 planar structure and, resultantly, its conductivity because of the closeness of the sizes of boron and carbon. The lattice parameters are moderately changed due to B—C bond (1.50 Å) being longer than the C—C bond (1.40-1.42 Å) in pristine graphene.[247,248]

The synthesis of B-doped graphene using pure graphite at high temperature (>2000°C) normally results in substitutional doping. However, when using GO at lower temperature (900°C-1200°C) produces more complex material with several different functional groups such as substitutional boron, borinic, borinic ester, boronic acid, and organo-borane (Figure 5).[245] Tuning the level of boron doping in graphene induces different bandgaps of B-doped graphene from 0 to 0.54 eV.[249] Boron doping can induce more holes to the valence band of graphene which further enhances the carrier concentration in B-doped graphene (0.5 carriers per dopant).[147,250,251]

The most frequently used methods range from solid state reaction (gas-solid reactions),[251,252] liquid state reaction (hydrothermal/solvothermal synthesis)[253,254] to high temperature (CVD).[255,256] These techniques can be split into top-down and bottom-up approaches. In the bottom-up approach, the arrangement of smaller components is more complex. For example, an atom can be assembled into molecules and molecules into nanostructure. This arrangement is achieved by covalent or non-covalent bonding. Top-down approach often uses microfabrication and nanofabrication methods whereby externally controlled tools are employed in the breaking down of the single crystal (bulk material) into an aqueous form or powder for production of nanomaterials.[257] Irrespective of the approach adopted, preparation of B-doped graphene requires a boron precursor and carbon precursor (graphite, GO, or rGO).

TABLE 3 Synthesis methods of N-doped graphene and their nitrogen concentration

Synthesis Method	Precursors	Nitrogen Content/%	Ref.
Thermal treatment	N^+ ion-irradiated graphene, NH_3	1.1	218
	GO, NH_3, argon	2.0-2.8	219
	GNR, NH_3	~2	220
	GO, melamine	7.1-10.1	222
	GO, amide/amine	10.9-13.4	223
Arc discharge	Multilayer graphene sheet, NH_3	1	152
	Graphite, NH_3, H_2, He	1	228
	Graphite, pyridine, H_2, He	0.6	228
	Nanodiamond, pyridine, He	1.4	228
CVD	Cu foil on Si substrate, CH_4, NH_3	1.2-8.9	205
	Cu foil, 1.3.5-triazine	2.1-5.6	208
	Cu foil, acetonitrile	~9	233
	Cu foil, pyridine	~24	234
	Cu foil, C_2H_4, NH_3	0-16	240
	Cu foil, CH_4, CO $(NH_2)_2$	3.72	241
	GO, melamine gel mixture	2.48	242

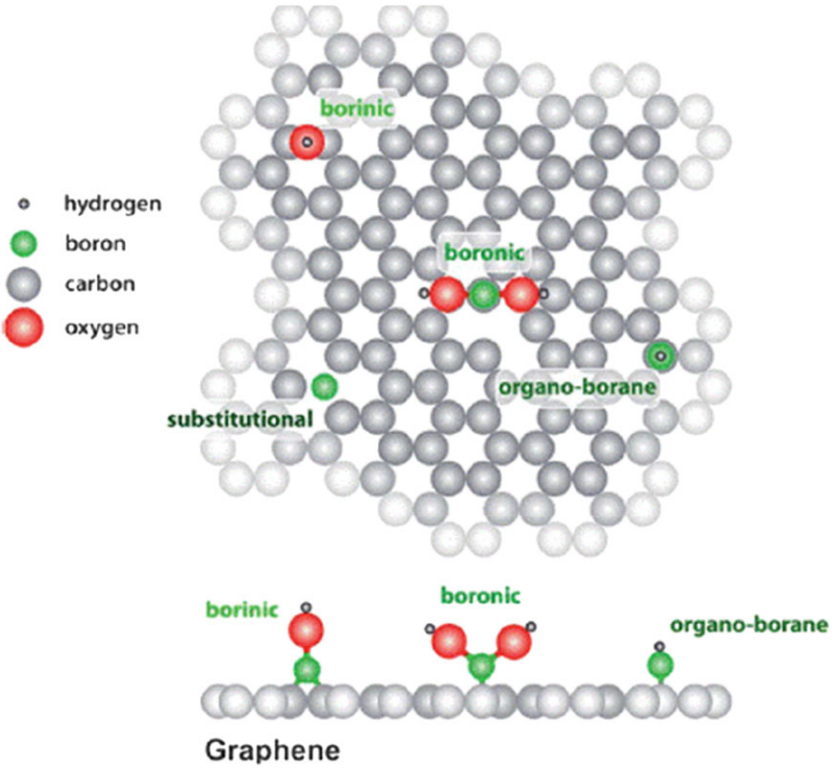

FIGURE 5 Ball model of B-doped graphene exhibiting the boron induced defects[245] [Colour figure can be viewed at wileyonlinelibrary.com]

In the solid-state synthesis, Panchakarla et al[258] were the first group to successfully dope graphene with boron. They used two methods during the synthesis of B-doped graphene. In the first method, B-doped graphene was synthesized using the arc discharge with graphite electrodes in the presence of different gases such as helium, hydrogen, and diborane. In the second method, B-doped graphene was synthesized by boron-packed graphite electrodes (3% B) with H_2 and He gases using arc discharge. The XPS revealed that boron was bonded to sp^2 carbon network. The level of doping was found to be about 1.2% to 3.1% which was slightly different from 1.0% to 2.4% given by electron energy loss spectroscopy used for confirmation. The Raman spectroscopy showed that the intensity ratio of D-band and G-band (I_D/I_G) of B-doped graphene was higher than the I_D/I_G ratio of undoped graphene and the G-band of B-doped graphene shifted to higher frequency.[258] This shift was attributed to boron doping. In a case where B-doped graphene is synthesized at a lower growth temperature (900°C-1200°C), different boron configurations such as boronic acids, boronic, and borinic esters (Figure 5) are produced.[258]

In 2016, Shaobo et al[259] reported boron doped reduced GO (B-rGO) synthesized from a facile dielectric barrier discharge (DBD) plasma approach using boric acid as a boron precursor under ambient conditions. The boron content in B-rGO was found to be 1.4%. Most reported B-doped graphene makes use of boron precursors, boron tribromide or diborane, which are toxic and require special handling procedures. However, a greener approach has been demonstrated by Sheng et al.[260] These authors employed less toxic boron trioxide vapour which was heated at temperature of 1200°C. The frequently used method for synthesis of B-doped graphene is based on solid state reaction between GO and boron trioxide or boric acid.[260,261] The materials are thermally annealed at a temperature between 900°C and 1200°C in inert argon atmosphere. Typical doping levels obtained have been shown to range between 0.5% and 10% on photoemission spectroscopy measurements.[260] More recently, a high-quality B-doped graphene was synthesized from SiC(001) single crystal by sublimation method. However, the boron content was very low (0.1%).[262]

Hydrothermal/solvothermal reaction approaches have been extensively used for doping of graphene.[253] This approach tends to produce graphene materials with surface and morphology functionalization. Lu et al[147] investigated a novel approach: Wurtz-type reductive coupling reaction without the use of a transition metal catalyst. In this approach, B-doped graphene was synthesized by reacting tetrachloromethane, metallic potassium, and boron tribromide at temperatures between 150°C and 210°C for 10 minutes in a closed securely teflon-lined stainless-steel autoclave (solvent thermal process). The

boron content in B-doped graphene was found to be 2.5%[147] when the XPS intensity measurement was used to quantitate atomic composition.

Comparatively, B-doped graphene is mostly synthesized using CVD approaches, and similarly, to N-doped graphene, Cu and Ni foils are used during the synthesis process. The boron precursors used can be liquid, solid, or gaseous. Gaseous boron precursors that have been investigated are 4-methoxyphenylboronic acid,[256] diborane,[250] and carborane.[263] Cattelan et al[264] reported boron-doped graphene which had been synthesized using polycrystalline copper as a substrate, diborane, and methane as boron precursor and carbon precursor, respectively. The synthesis was carried out at a growth temperature of 950°C, and the boron content that was obtained was 2.5%.[264]

Wu et al[265] reported boron doped single layer graphene synthesized on copper at growth temperature of 1000°C in an argon carrier using CVD technique. Boric acid and polystyrene were employed as boron and carbon precursors, respectively. Under these conditions, the obtained B-doped graphene had boron content of about 5%. When a solid boron precursor such as phenylboric acid produced large monolayer polycrystalline graphene film from the CVD on copper foils under hydrogen gas stream at 950°C.[266] Other boron precursors include triphenylborane, boron trioxide, and ammonia borane.

6.5 | Sulfur-doped graphene

Sulfur can be substitutionally doped into graphene framework to modulate chemical and electronic properties of graphene. Its bonding configuration is similar to that of oxygen; unlike nitrogen and boron doping effect, sulfur doping induces a negligible charge transfer that occurs in the C—S bond due to similar electronegativity between carbon ($\chi = 2.55$) and sulfur ($\chi = 2.58$). Figure 6 exhibits the different configuration being, C—SH, C—S—C, and C—SO_x—C (where x = 2, 3, or 4).[268] The C—C bond length is shorter than that of C—S bond (1.78 Å)[269]; hence, sulfur doping tends to provide a stable structure. It has been reported that the sulfur doping in graphene takes place in two steps, firstly, formation of defect sites, secondly, double bond S═S rapture and the end-product (graphene sheet) change into a small-bandgap semiconductor or becomes more metallic compared with pristine graphene.[270] The two bands in the Fermi level are lifted in the band plot of sulfur-doped graphene (S-doped graphene) with one sulfur atom. This results in a bandgap of 0.3 eV with one S atom whereas containing two S atoms causes an increase in the metallic properties of graphene. S-doped graphene sheets are more resistive and more metallic as compared with pristine graphene. They are more resistive because of the sulfur and oxygen functionalities which causes the free carrier trapping.

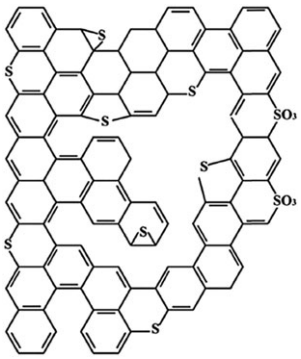

FIGURE 6 Bonding configuration of S-doped graphene[267]

Recently, various methods have been used in the synthesis of S-doped graphene. Sulfur atoms can be inserted into the graphene frameworks using CVD and thermal annealing of GO.[271] The sulfur-containing porous carbon material has been synthesized using infiltration of the carbon source into zeolite pores by means of impregnation and CVD approach.[272] Thermal treatment approach has been successfully employed in the synthesis of S-doped graphene whereby graphene or GO is treated with sulfur dioxide,[273] benzyl disulphide,[268] hydrogen disulphide,[274] and carbon disulphide.[275] These studies have shown that the thermal treatment approach produces a low sulfur content, even when the treatment temperature has been adjusted.[276] Poh et al[273] reported that S-doped graphene is highly dependent on the type of sulfur precursor and type of graphite oxide or graphene used during the synthesis.

Xu et al[169] reported that the CVD method can be used to synthesize S-doped graphene using thiophene as sulfur precursor. The XPS analysis revealed that there was about 3.2% of sulfur content in S-doped graphene. However, Gao et al[277] reported the synthesis of large-area S-doped graphene using Cu substrate and hexane in the presence of sulfur *via* CVD approach. Yet, the sulfur content was very low, approximately 0.6%. Yang et al[268] synthesized S-doped graphene *via* thermal annealing of GO and benzyl disulphide as sulfur source. At different annealing temperatures of 600°C, 900°C, and 1050°C, sulfur contents of 1.53%, 1.35%, and 1.30% were obtained, respectively.[268] This shows that the annealing temperature affects the doping levels and lower temperatures tend to produce higher sulfur content. However, in 2015, Liu et al[278] reported the use of similar sulfur containing precursor (benzyl disulphide) and GO in the synthesis of S-doped graphene using microwave-assisted solvothermal method and achieved a doping level of 2.3%. Liang et al[274] reported the S-doped graphene that had been

annealed at a temperature of 1000°C with gaseous sulfur source of H_2S gas on Si/SiO_2. Since then, different liquid organic material precursors such as hexane have been also employed in the presence of sulfur when CVD method is used together with copper substrate.[277] Hassani et al[271] reported a high sulfur doping level of 5% (XPS) that was grown from CVD and sulfur powder as sulfur precursor. Thus, the level of sulfur in S-doped graphene varies with synthetic technique and sulfur-containing precursor used.

6.6 | Phosphorus-doped graphene

Phosphorus can also be used as a dopant and precursor to dope graphene. It belongs to group 15 elements below nitrogen. However, it is larger than nitrogen. Therefore, its doping causes greater structural distortion. The electronegativity of phosphorus ($\chi = 2.19$) is lower than of carbon ($\chi = 2.55$) which demonstrates higher electron donating ability.[279] Phosphorus, although iso-valent to nitrogen, has different doping effect due to higher electron-donating ability and more diffuse valance orbitals ($3s^2\ 3p^3$).[280] Consequently, the polarity of C—P bond is different from that of C—N bond, and this may be due to the more diffuse valance orbitals of phosphorus.[281]

The large atomic radius of phosphorus does not appear in-plane of graphene[282] which significantly affects the bandgap phosphorus-doped graphene (P-doped graphene). Theoretically, the bandgap (0.53 eV) of P-doped graphene is higher than those of both N-doped graphene (0.14 eV) and B-doped graphene (0.14 eV). Interestingly, doping with phosphorus is easier than with nitrogen since the formation energy of P-doped graphene is 7.1 eV/atom[269] while that of N-doped graphene is 8.0 eV/atom.[228] This suggests that the phosphorus doping is energetically favourable.

During doping, phosphorus can form a pyramidal-like bonding configuration along with three carbon atoms.

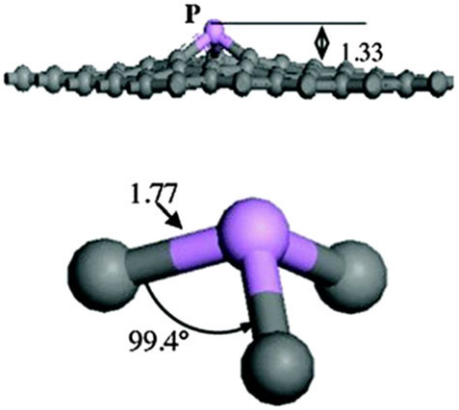

FIGURE 7 Geometric structure of P-doped graphene[283] [Colour figure can be viewed at wileyonlinelibrary.com]

This is due to strong hybridization between carbon 2p and phosphorus 3p. This is due to the change of hybridization of carbon from sp^2 to sp^3.[283] In pyramidal-like bonding configuration, the phosphorus overhangs from graphene plane and the P—C bond length (1.33 Å) increases by 24.6% compared with C—C bond length of pristine graphene (Figure 7).[283] Some and co-workers[284] reported the synthesis of highly air-stable P-doped graphene that constituted n-type behaviour. Recently, various techniques for substituting phosphorus atom in the lattice of graphene have been investigated and reported such as CVD and inductively coupled plasma, and the most effective method is microwave plasma.[285,286]

Zhang et al[287] reported that P-doped graphene synthesized using triphenylphosphine as phosphorus precursors and graphite oxide as carbon *via* thermal treatment resulting in a phosphorus content of 1.81% on XPS measurement. The P-doped graphene have also been synthesized using post-thermal annealing of graphene/GO with triphenylphosphine as a P-containing precursor under a protecting atmosphere.[287,288] Some et al[284] reported that the P-doped graphene prepared from triphenylphosphine under argon at 100°C to 250°C yielding phosphorus content of 4.96%. Similar phosphorus-containing precursors were employed in the synthesis of P-doped graphene by Shin et al[289] using inductively coupled plasma technique to yield phosphorus content of 2%.

Ionic liquids such as 1-butyl-3-methylimidazolium hexafluorophosphate have been employed in the synthesis of thermal annealed P-doped graphene as phosphorus precursor.[290] During the thermal annealing process, different covalently bonded tetrahedral structures such as C_2PO_2, C_3PO, and CPO_3 were observed and consequently resulting in a charge redistribution in P-doped graphene. Dennis[291] reported that the bandgap opening relies purely on phosphorus doping level, eg, 0.5% resulted in a bandgap of 0.3 to 0.4 eV. In situ synthesis of P-doped graphene has been reported by Latorre-Sanchez et al[292] where a pyrolysis of natural alginate and dihydrogen phosphate ion was done under oxygen at a temperature of 900°C. The P-doped graphene obtained had P—C and P—O bonds and an optical bandgap of 2.85 eV. It should be noted that P-doping gives rise to a magnetic moment ascribed to unpaired electron spin.

6.7 | Halogen-doped graphene

Halogen (group 17 elements, namely, fluorine [F], chlorine [Cl], bromine [Br], and iodine [I]) are well known for their higher reactivity compared with other elements from groups 13 to 16. When the halogen is doped on the graphene lattice, it converts the sp^2 carbon bonding

into a sp^3 state, which produces drastic distortions in the electronic and geometric structures of graphene.[293] It also enhances the active site of graphene, which modifies the graphitic carbon material, enabling doped graphene to be applied in various technological fields, namely, stem cells,[294] photo-catalytic,[295] DSSCs,[296] and ORR.[293] Halogen-doped graphene is widely applied as an electrocatalyst for ORR in fuel cells. However, very few studies have been reported on its application in DSSCs.

The most reactive element of the halogen is fluorine. When F is bonded to graphene, it results in strong F—C bonds and the C—C bond length stretches between 1.57 and 1.58 Å.[297] The fluorine bonding causes an increase in hydrophobicity of graphene.[298] Doping with Cl results in longer bond length and lower binding energy than H and F. This indicates that the covalent bond (Cl—C) is less stable compared with the C—H and C—F bonds.[299] Chlorine-doped graphene is reported to be thicker (1.1-1.7 nm) than fluorine-doped graphene due to the longer bond length.[299] There are very few experimental and theoretical reports on bromine-doped graphene and iodine-doped graphene because of the thermodynamic instability related with their low electronegativity (F = 3.98, Cl = 3.16, Br = 2.96, and I = 2.66) and large sizes. Br and I tend to interact with graphene by physisorption without interrupting the sp^2 carbon network.[300]

Halogen-doped graphene can be synthesized by ball milling,[301] arc discharge,[298] and microwave plasma[302] approaches. These approaches tend to produce differing doping levels of halogen-doped graphene. Halogen-doped graphene nanoplates were prepared by the ball milling approach in the presence of I, Br, and Cl.[301] A decrease in halogen doping level of the halogen-doped graphene nanoplates was observed (Cl—5.89%, Br—2.78%, and I—0.95%) due to the size and chemical reactivity of these elements. The arc discharge approach has been employed in the synthesis of fluorine-doped multi-layered graphene sheets which contained about 10% of F.[298] Bouša et al[302] reported chemical modification of graphene by using various aryl halogens to produce halogen-doped graphene *via* the microwave plasma approach. XPS analysis revealed the successful covalent bonding of aryl molecules to the graphene basal plane. Different halogen doping levels were obtained; fluorine-doped graphene (5.06%) was reported to contain higher doping levels than chlorine-doped graphene (4.76%), bromine-doped graphene (3.86%), and iodine-doped graphene (3.50%).

6.8 | Co-doped graphene

Previous studies had shown that heteroatoms can be co-doped in the synthesis of CNTs. Similar to CNTs, graphene can also be co-doped with multiple species of foreign atoms. The co-doping of heteroatoms produces synergistic effects and create new properties. Heteroatoms such as boron and nitrogen have similar size but generate opposite doping effects.[303] N, B co-doped graphene can be achieved by using two precursors (nitrogen and boron precursors) or a precursor that contains both nitrogen and boron in its structure. When they are simultaneously doped on graphene, they form boron nitride because of the phase separation between carbon and boron nitride.[237,304] This is ascribed to the larger binding site of C—C and B—N bonds as compared with that of N—C and B—C bonds. Co-doping of boron and nitrogen produces different bonding configuration and bond lengths, eg, C—B (1.49 Å), C—N (1.35 Å), C—C (1.42 Å), and B—N (1.45 Å).

Figure 8 depicts the top views of five different structures, being pristine graphene, N-doped graphene, B-doped graphene, hexagonal boron nitride (h-BN), and boron and nitrogen co-doped graphene. The h-BN is well-known as white graphene. It is a dielectric which consists of a wide bandgap of approximately 5.9 eV. h-BN is synthesized in a similar way to other doped graphenes by using CVD method. As-synthesized h-BN exhibits larger optical energy (5.5 eV) and elastic modulus (200-500 N m^{-1}).[305] Boron and nitrogen co-doped graphene is more thermally stable than B-doped graphene, however, less thermally stable when compared with N-doped graphene.[305]

The co-doping tends to enhance the band gap due to symmetry breaking.[304] Both nitrogen and boron produce a bandgap at the Dirac point; however, they shift the Fermi level in different directions.[304] B, N co-doping is presumed to create a bandgap only at the Dirac point with no shifting in the Fermi level.[76,246] Various methods have been used in the synthesis of N- and B-doped graphene. Ci et al[77] reported dual N and B co-doped graphene synthesized *via* CVD approach from ammonia borane and methane as the boron, nitrogen, and carbon precursors, respectively. The doping level was tuned by altering the reaction parameters. The N, B co-doped graphene with a high doping level normally has large area and N-B hybridized domain as demonstrated by XPS studies.[77] Hydrothermal approach has been reported by Wu et al[306] where N, B co-doped graphene was synthesized using ammonia borane and GO, which resulted in nitrogen content of 3.0% and boron content of 3.0%. In 2013, Bepete et al[307] reported the incorporation of small BN domain (0.3%-0.5%) using nitrogen gas and boric acid as nitrogen and boron precursors.

Co-doping with multiple species of foreign atoms produces different bonding configurations. Co-doping of phosphorus causes a pyridinic bonding of nitrogen on

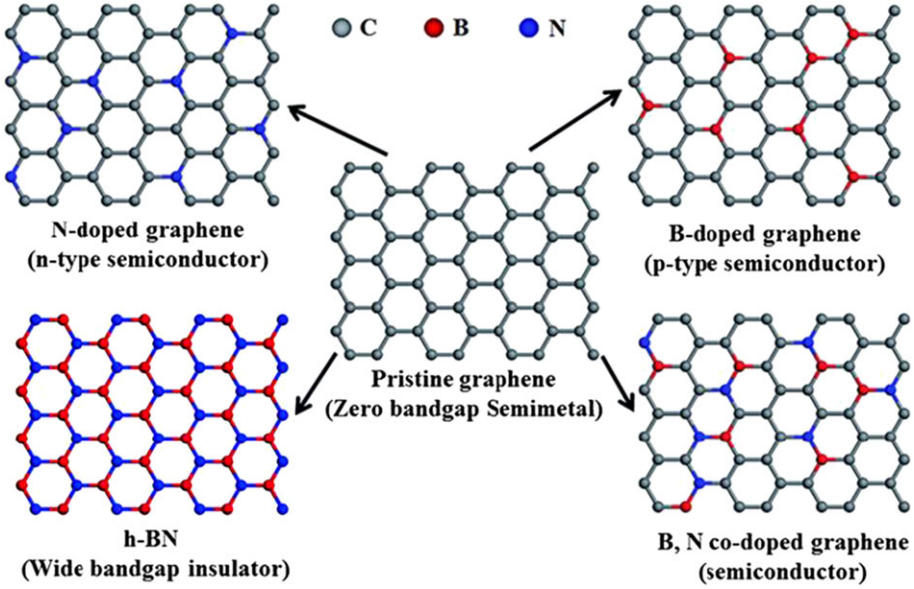

FIGURE 8 Schematic diagram of pristine graphene, N- and B-doped graphene, h-BN and B, N co-doped graphene[305] [Colour figure can be viewed at wileyonlinelibrary.com]

graphene[308] while the co-doping of sulfur promotes graphitic-N as dominant.[169] Porous P, N co-doped graphene has been synthesized using magnesium oxide-templating in situ CVD approach with methane and ammonium phosphate as nitrogen and phosphorus precursors.[309] The XPS analysis indicated phosphorus and nitrogen co-doped graphene formed had nitrogen content of 2.6% with different nitrogen atoms configuration of pyrrolic-N, pyridinic-N, and graphitic-N; however, the phosphorus content (0.6%) was found to be less than that of nitrogen. The phosphorus atoms were covalently bonded with carbon in the various tetrahedral forms, being, C_2PO_2, C_3PO, and CPO_3. The level of doping and configuration of P and N co-doped graphene are affected by synthesis temperature in the CVD approach.[310] The synthesis temperature of 700°C produced different nitrogen species in the sequence: pyridinic-N > pyrrolic-N > graphitic-N. P and N co-doped graphene synthesized at 800°C and 900°C had similar nitrogen species of pyrrolic-N and graphitic-N while those obtained at 1000°C exhibited a graphitic-N. Higher temperature enhanced the number of phosphorus-carbon bonds and decreases the number of phosphorus-oxygen bonds. The increase in doping effect is due to the formation of more-stable bond configurations. However, the doping levels for both nitrogen and phosphorus decrease as the temperature increases.

Co-doped graphene-based materials potentially have promising properties for different applications. Very few reports exist on graphene that is simultaneously doped with nitrogen and sulfur.[311] Wang et al[312] reported the interaction between sulfur and nitrogen in co-doped graphene. In their work, N and S co-doped graphene was prepared by means of one-pot hydrothermal approach using amino acid and ly-cysteine as nitrogen and sulfur doping agents. The concurrent incorporation of nitrogen and sulfur atoms in the presence of oxygen alters the surface chemistry of carbon causing the increase in doping levels, whilst direct bonding between nitrogen and sulfur atoms was not fully demonstrated.[312] Xu et al[169] reported N, S co-doped graphene synthesis from a nitrogen source of pyrimidine and sulfur source of thiophene at low temperature. The doping level of S and N atoms was found to be 0.7% to 2.0% and 3.7% to 5.7%, respectively. The use of multi-precursors is most easily controllable and convenient than single precursor doping methods. The N, S co-doped graphenes are applied in lithium ion batteries,[313] supercapacitors,[312] and electrocatalytic ORRs[314,315] and exhibit promising performance.

7 | DSSCs

Most research has been focusing on open-circuit voltage (Voc), boosting the short-circuit current density (Jsc), and fill factor (FF) to increase the efficiency of the cells. Enhancing the CE material causes the FF of the cell to increase, which is generally affected by the cell series resistance (Rs) and the slope of the tangent line to the current density (J)-voltage (V) curve at Voc.[309] The charge carrier's transportation from the photoanode to the CE encounters varying resistance. The dominant charger transfer in DSSCs is at the CE/electrolyte interface. At

the CE/electrolyte interface, the charge-transfer resistance and series resistance are subjugated to the CEs. The series resistance of a solar cell dominates FF losses. A higher FF is due to smaller series resistance which generate higher power conversion efficiency.

7.1 | Doped graphene as a counter electrode for DSSCs

The CE is used to minimize redox species in DSSCs, which act as mediators during the regeneration of the sensitizer occurring after electron injection. CEs are required to have good catalytic activity to enhance the reduction of the electrolyte, hence should have lower sheet resistance, low cost, and high thermodynamic stability.[316] The reactions occurring at the CEs are highly dependent on the nature of the redox mediator being used for charge transfer between the CE and photoelectrode.[316-318]

7.1.1 | Oxygen-doped graphene in DSSCs

Graphene oxide and rGO as a CE are reported to have good electrocatalytic ability in reducing the redox couple in DSSCs.[93] This is because they possess structural defects and oxygen-containing functional groups, for example, carbonyl, epoxide, and hydroxyl.[319] It was observed that the fabrication procedure of GO can also be regarded as a major factor in determining the performance of GO in DSSCs. DSSCs with graphene-based CE exhibited higher power conversion efficiency of approximately 90% compared with platinum-based CE.[316] Kavan et al[320] demonstrated that increasing the number of oxygen-containing groups results in increase in catalytic activation. Therefore, different materials of GO used in various procedures produced different power conversion efficiency. DSSCs fabricated from GO have been reported by Kumar[321] which produce a higher conversion efficiency of 5.58%. Recently, various researchers reported a reduction of GO to rGO chemically,[322] thermally,[323] electrochemically,[324] and photothermally[325] and their application as GO or rGO-based CEs, exhibiting that rGO could be a better potential candidate for fabricating flexible and Pt-free DSSCs. Jang et al[326] reported the use of rGO as CE that had been developed from spin coating. This method resulted in a uniform morphology of rGO and high particle size, producing a power conversion efficiency of 3.99%.

Yeh et al[192] investigated the effect of using GO and highly conductive rGO as CE. Highly conductive rGO yielded higher power conversion efficiency of 7.62% compared with a GO (0.03%). Highly conductive rGO exhibited a good electrocatalytic ability than GO because of its high standard heterogeneous rate of redox couple reduction and its electrochemical surface area. Recently, Sarker et al[327] developed a high efficiency DSSC with rGO as CE synthesized by doctor-blading a viscous rGO on FTO substrate. The DSSC-rGO electrode exhibited similar catalytic performance as platinum-based cell showing promising characteristics of replacing Pt.

7.1.2 | Nitrogen-doped graphene in DSSCs

N-doped graphene has been employed in DSSCs for harvesting energy. N-doped graphene has exhibited gigantic electrocatalytic activity due to high charge polarization that occurs due to difference in electronegativity between nitrogen and carbon.[328] It has been reported that N-doped graphene possesses a good electrocatalytic activity and high conductivity that are able to produce a conversion efficiency of more the 5% (Table 4). Metal-nitrogen-doped graphene or metal-free nitrogen graphene has been used as CE.

Xue et al[329] demonstrated that the use of (3D) N-doped graphene (nitrogen content of 7.6%) synthesized from freeze-drying of GO under ammonia gas treatment on DSSCs as a CE with a N719 as a dye sensitizer and I_3^-/I^- redox couple. It provided a power conversion efficiency of 7.07%. However, DSSCs had a poor FF of 0.58. The efficiency was slightly lower than that of platinum-based CEs because of the low FF.[329] This is due to the fact nitrogen doping approaches that include low-pressure drying and high-pressure synthesis. Further, ammonia gas treatment is toxic; therefore, it is not suitable for mass production. However, N-doped graphene sheets which were synthesized in a similar method (hydrothermal reduction of GO) and similar nitrogen precursor (ammonia) was reported by Wang et al.[330] These N-doped graphene sheets had a nitrogen content of 2.5%. The

TABLE 4 Energy conversion efficiency for DSSCs with N-doped graphene as a CE

Counter Electrode	Jsc, mA cm^{-2}	Voc, V	FF	ŋ, %	Ref.
N-GR foam	15.84	0.77	0.58	7.07	329
N-GR	10.55	0.82	0.55	4.75	330
N-GR	12.32	0.71	0.60	6.12	331
Nanoplatelet-N-GR	14.02	0.89	0.74	9.05	332
N-GO/Pt	14.10	0.75	0.74	9.38	333
NGnP5	14.78	0.97	0.72	10.27	332
FeN/N-GR	18.83	0.74	0.78	10.86	334
N-GR	16.13	0.73	0.74	8.71	334
N-GR	13.43	0.64	0.59	5.07	335

N-doped graphene CE was created by drop casting a N-doped graphene sheet solution onto FTO glass substrate and the redox couple used was I_3^-/I^- redox couple. This DSSC produced a conversion efficiency of 6.12%.

In 2013, Shaocong et al[331] demonstrated that doping graphene with nitrogen can enhance the power conversion efficiency of DSSCs (5.4%—N-doped graphene) whilst 5.1%—Pt, improves catalytic activity and lowers the charge transfer resistance. They further demonstrated that N-doped graphene doped at different temperatures and increasing the nitrogen content have no effect on the power conversion efficiency. The state of nitrogen doping was observed to play a major role in catalytic activity. Jeong et al[151] found that pyrrolic-N has large binding energy toward ions in the solution, which may result in difficulty in the desorption of I^* to I^- for iodine reduction reaction. Thus, the decrease of reaction sites would restrict the overall activity.

Yen et al[332] reported a power conversion efficiency of 4.75% which was achieved when N-doped graphene prepared from the hydrothermal method was used as a CE in DSSCs. Later that year, nanoplatelet-NGR were employed as CE in DSSCs, and they produced a power conversion efficiency of 9.05% and FF of 0.74, yet a different redox couple of Co $(bpy)_3^{3+/2+}$ and dye sensitizer of O-alkylated-JK-22 were used.[333] Graphene nanoplatelets doped with nitrogen at the edge which are synthesized from ball-milling method have been investigated.[334] The investigation was performed using six different NGnP/FTO CEs, NGnP1, NGnP2, NGnP3, NGnP4, NGnP5, and NGnP6 that have been fabricated from different deposition times, 2, 3, 5, 7, 9, and 11 minutes, respectively.[334] The NGnP CEs displayed excellent electrocatalytic performance for the redox couple (Co $(bpy)_3^{3+/2+}$) with lower charge transfer resistance.[334] As the deposition time increased, the energy conversion efficiency also increased. However, at the deposition time of 11 minutes a decrease in efficiency was experienced. The highest power conversion efficiency of 10.27% was obtained from NGnP5.[334]

Metal-nitrogen-doped graphene CE produces a higher power conversion efficiency than metal-free nitrogen doped graphene. Lin et al[335] achieved an efficiency of 9.38% when N-doped graphene was used on Pt-sputtered FTO substrate (NGR/Pt/FTO) as CE. This high efficiency was caused by the electron transfer effect which was supplied by NGR and light-reflection effect from NGR/Pt/FTO which promoted the electron transfer from CE to the electrolyte (I_3^- ion) and light. In 2015, Xue et al[336] report N-doped GNRs (nitrogen content of 6.5% with a surface area of 751 $cm^2\ g^{-1}$) which was synthesized from thermal treatment of GO nanoribbons in ammonia gas produced power conversion efficiency of 5.07%.

Kim et al[337] demonstrated that treating N-doped graphene with TiO_2 produced a power conversion efficiency of 9.32%. This is because the graphene/N-doped TiO_2 composite expands the absorption into the visible light region and increases the rate of electron transfer.[337] When N-doped graphene nanosheets with transition metal nitrides (iron nitride) core-shell nanoparticles are employed as CE material that exhibited a power conversion efficiency of 10.86% which was greater than that of DSSCs with platinum or N-doped graphene as CE being 9.93% or 8.715%, respectively.[338] In 2017, Yang et al[339] reported that the electrochemical measurements of nitrogen-doped holey graphene exhibited better electrochemical stability and higher catalytic activity with respect to those of Pt, and DSSCs with optimized nitrogen-doped holey graphene demonstrate a power conversion efficiency of 9.07%, which was higher than efficiency of 8.19% for Pt as the CE.

Recently, N-doped graphene on a Pt-sputtered FTO substrate (NGR/Pt/FTO) as CEs achieved an efficiency of 9.38% *via* attributed to firstly, hole-cascading transport at the interface of electrolyte/CEs, as a result of controlling the valence band maximum of I^-/I_3^- redox couple and the Fermi level of Pt by nitrogen doping. Secondly, the extended electron transfer surface effect provided by large-surface-area doped graphene. Thirdly, the high charge transfer efficiency due to superior catalytic characteristics of N-doped graphene. Finally, the superior light-reflection effect of NGR/Pt/FTO CEs, facilitating the electron transfer from CEs to I_3^- ions of the electrolyte and light absorption of dye.[340] This lessens the loss that occurs at the interface of electrolyte/CE and cause an increase in power conversion efficiency of DSSCs.[246]

7.1.3 | Boron-doped graphene in DSSCs

In the meantime, there have been few reports based on application of B-doped graphene as CE in DSSCs. Fang et al[261] reported the use of B-doped graphene as CE in a DSSC which is based on an I_3^-/I^- redox couple. The B-doped graphene was fabricated from annealing of boron trioxide with GO at a temperature of 1200°C for 4 hours and resulted in a boron content of 1.0%.[261] This provided a high-power conversion efficiency of 6.73%.[261] The application of B-doped graphene as a CE with the Co(2,2-bipyridine)$_3^{2+/3+}$ redox couple was reported to produce a higher power conversion efficiency than a I_3^-/I^- redox couple.[341] B-doped graphene exhibited higher electrocatalytic activity than Pt as CE in Co $(bpy)_3^{2+/3+}$ redox couple.[341] Generally, B-doped graphene exhibits good electrochemical stability[341,342] and lower charge-transfer resistance.[343] DSSCs developed from B-doped graphene

produced a power conversion efficiency of 9.21% which was higher than that of platinum CE (8.45%).[341]

7.1.4 | Sulfur-doped graphene in DSSCs

Sulfur-reduced GO (SRGO) has been applied in DSSCs to produce a power conversion efficiency of 4.23%.[344] The SRGO has been fabricated from the one-step synthesis using hydrothermal process with the use of mercaptoacetic acid. It had a sulfur content of 5.45%.[344] Meng et al[345] reported the use of sulfur-doped porous graphene (SPG) in DSSCs as CE. SPG was synthesized from sulfur powder and poro-foaming agent *via* thermal annealing approach (800°C, 900°C, and 1000°C). The annealing approach (especially, higher temperature – ≥ 900°C) showed a better photovoltaic and electrochemical performance. A high-power conversion efficiency of 8.67% was achieved when as-made SPG was used as CE, outperforming the Pt (7.88%). Sulfur atom can tune the electronic structure of graphene and create a highly active site with a low change in carbon conjugation length. In 2017, Mustafa et al[346] presented a new CE that consists of GO doped with poly(3,4-ethylenedioxythiophene) and TiO_2. Hence, a power conversion efficiency of 1.166% was achieved. The incorporation of poly(3,4-ethylenedioxythiophene)/GO (PEDOT-GO) with TiO_2 was found to produce more promising results than platinum CE (0.727%).

7.1.5 | Phosphorus-doped graphene in DSSCs

P-doped graphene has been mostly applied in fuel cells,[347] Li-ion batteries,[287] and supercapacitors[348] as an electrode. Wang et al[349] were the first to demonstrate that P-doped reduced GO can be employed as CE in DSSCs with I^-/I_3^- redox couple, and it produced a power conversion efficiency of 6.26%. Ahn et al[350] demonstrated that phosphorus doped 3D graphene provides better performance than platinum as CE. P-doped 3D graphene produced a power conversion efficiency of 8.46% which was higher than that of platinum (6.01%). However, in 2017, Xu et al[351] reported the higher power conversion efficiency of 7.08% fabricated from P-doped porous graphene nanosheet with I^-/I_3^- redox couple. P-doped graphene nanosheet was synthesized using CVD method, and it had a surface area of 1627.8 $m^2\ g^{-1}$.[351]

7.1.6 | Halogen-doped graphene in DSSCs

Recently, Jeon et al[352] demonstrated that edge-selectively halogenated graphene nanoplatelets (XGnPs, X = Cl, Br, and I) and halogen contents of Cl, Br, and I in XGnPs as 3.18%, 1.77%, and 0.66%, respectively, used as CEs indicated enhanced electrocatalytic activities toward Co $(bpy)_3^{3+}$ reduction reaction in DSSCs with an exceptional electrochemical stability. These authors further reported IGnP-CE to have the lowest charge-transfer resistance (Rct) of 0.46 Ω cm^2 at the CE/electrolyte interface. It should be noted that this value is much lower than that of Pt-CE (0.81 Ω cm^2). It was also noted that in DSSCs with IGnP-CE had the highest FF (71.3%) and cell efficiency (10.31%), whereas those of DSSCs with Pt-CE were only 70.6% and 9.92%, respectively. These characteristics could be inferred to emanate from an established balance between electrical conductivity for efficient charge transfer and charge polarization which enhances reduction activity of redox couples simultaneously.[353,354]

7.1.7 | Co-doped graphene in DSSCs

It has been reported that co-doping with two or more elements can generate a distinctive and synergistically increased electronic structure in the carbon matrix. It also causes an increase in electrocatalytic activity of graphene because of the increase in spin densities and asymmetries of charge at the various sites of the double-doped graphene. A power conversion efficiency of 8.08% which is superior to 6.34% of Pt-CE was achieved when GO was reduced and doped with nitrogen and boron.[166] This B and N co-doped graphene was reported by Yu et al[166] where the doped graphene was achieved *via* chemically grafting ionic liquid followed by thermal annealing.

Luo et al[344] reported a co-doping of nitrogen and sulfur atoms in graphene which was fabricated using DL-penicillamine which possesses both atoms in its structure. The NSRGO had nitrogen and sulfur contents of 2.12% and 8.92%, respectively. The power conversion efficiency of NSRGO was compared with RGO, SRGO, and NRGO. NSRGO was found to exhibit a higher power conversion efficiency of 4.73%.[344] This is because the co-doping of heteroatoms provides more electrocatalytic active sites to ease the charge transfer between the cathode/electrolyte interface which leads to higher catalytical performance and increase in photovoltaic performance.[344] However, a high power conversion efficiency of 7.42% had been demonstrated by Kannan et al[355] which was higher than that of a single atom-doped graphene (N or S-doped graphene CE). This high catalytic activity is ascribed to high charge polarization which produced the synergistic effect between the different electronegativities of carbon and nitrogen. Furthermore, the structural distortion is produced by the larger atomic size of sulfur. The bifacial DSSCs with high

transparent nitrogen-doped graphene, sulfur doped and nitrogen and sulfur dual-doped graphene-like carbon films as CEs exhibit dramatically enhanced power conversion efficiency (PCE) of 3.74%, 3.86%, and 4.22% under front-side illumination compared with that of pristine graphene as CE.[356] 3D N and S co-doped rGO was reported by Yu et al[357] with an efficiency of 9.40% which was higher than that of platinum (9.10%). The high electrochemical performance was due to the synergistic effect of nitrogen and sulfur atoms in graphene.

Nitrogen and phosphorus belong in the same family; therefore, they show higher electron-donating ability which further shows stronger n-type behaviour.[358] The defects induced by co-doping (N and P) is predicated to bring about a highly localized state which is close to the Fermi level, especially for electrocatalysis.[359] However, N and P-doped graphene can also be applied in DSSCs as metal-free electrocatalyst. Yu et al[360] reported the use of N and P-doped graphene and single-component N or P-doped graphene in DSSCs. They produced a better performance along with a conversion efficiency of 8.57% which was higher than that of single-element N or P-doped graphene CE.[360]

8 | DFT STUDIES

Most frequently, DFT calculations for DSSCs estimate the adsorption energies of atomic iodine under vacuum and explicit acetonitrile solvation conditions. Considering the pristine armchair and zigzag edges as well as the basal plane of graphene sheets, the I atom adsorption energies have been shown to be below the optimal range for the CE catalytic activity (−0.17, 0.17, and −0.49 eV, respectively).[361] Recently, edge models involving double-coordinated Se (C—Se—C) or oxidized Se atoms also failed to support I atom adsorption. But, the I atom binding criterion for CE has been shown to be effective for the single-coordinated Se-doping cases (C==Se), with adsorption energies of 0.77 and 0.48 eV for the armchair and zigzag edges, respectively.[361,362] For instance, the I_3^- /I^- ions have been shown to adsorb on the graphitic basal plane at distances of 3.18 to 3.37 Å.[361] This potentially possesses an n-type shift of the graphene band and significantly increases currents at finite bias voltages. It can, thus, be argued that although the graphitic basal plane cannot drive an iodine reduction reaction on its own it has good current-carrying capability, a necessary condition for high CE catalytic activity.

It is prudent to examine the dielectric function, absorption spectrum, and energy loss-function of a single layer graphene sheet based on the density functional calculations. It has been shown for light polarization parallel and perpendicular to the plane of the graphene sheet and compared with doped graphene, the available theoretical, and experimental results appear the same. For example, it has been found that individual boron and nitrogen doping does not significantly affect the imaginary dielectric function and hence the absorption spectra. However, there is a significant red shift in absorption towards the visible range of radiation at high doping for the B/N co-doping[361] of graphene.

9 | COMMERCIAL, COST, AND ENVIRONMENTAL PERSPECTIVES

The exponential raise in commercial applications of optoelectronic materials of organic and nanostructured electronic origin, coupled with environmental concerns, motivates the quest for lower cost approaches to sustainable electricity production. The present work examined DSSCs and specifically the use of heteroatom-doped graphene as a CE. This is a focussed interface engineering strategy that employs innovative nanostructures and interface processing to enhance device performance. There is limited literature on photochemical studies on the control of interface morphology, which complicates the determination of clear structure/function relationships in these very important devices. A number of strategies are under investigation to achieve control of the interface morphology in organic donor/acceptor films.[363] This has seen an increase in sophisticated approaches for the design and optimization of solid-state photovoltaic devices. However, technological concerns about shelf-life and device stability when using liquid electrolytes need to be addressed. Generally, DSSCs rely on photoinduced charge separation at a dye-sensitized interface between a nanocrystalline, mesoporous metal oxide electrode, and a redox electrolyte. They are potentially a low-cost solar energy conversion technology, but the challenge is achieving a rational optimization of materials and device designs.[364] The success of graphene-based materials used for energy applications wholly depends on the development and optimization of production methods. Of great interest is the optimized control the sheet size and increasing the edge-to-surface ratio, which is vital for optimizing electrode performance in fuel cells and batteries. The frequently employed DSSC materials such as TiO_2 are inexpensive, easily available, and safe to the environment. The raw materials are less prone to contamination and processable at ambient conditions, thus upscaling of manufacturing processes for mass production is even easier. The better performance of DSSCs under lower light intensities makes them appealing for

indoor applications, a major driver for any commercialization effort.[365,366]

10 | CONCLUSION

In summary, heteroatom-doped graphene materials have been investigated as efficient CEs for DSSCs. DSSCs show significant opportunities to the researches in renewable energy. In the DSSCs, the CE has good electrocatalytic activity and high electrical conductivity which is responsible for collection of electrons from the external circuit and for catalysing reduction reactions. Therefore, alternative CEs such as graphene and heteroatom-doped graphene that are low-cost are preferentially used instead of high-cost platinum CEs. From the aforementioned studies, various heteroatom-doped graphene has revealed promising perspectives as CEs in DSSCs. Heteroatom-doped graphene as CE demonstrated significantly higher power conversion efficient compared with platinum-based CE. Enhanced efficiency is due to improved electron transfers and dissociation of excitons at electrodes

Various power efficiency has been achieved from 2008 to 2018, depending on the heteroatom employed in the CE. To our knowledge, the efficiency of DSSCs depends on how the CE has been fabricated. When graphene is doped with heteroatoms such as O, N, B, S, and P modulation of electronic properties of graphene is observed. Heteroatom doping provides graphene with different structural, physicochemical, electromagnetic, and optical properties. The heteroatom-doped graphene properties depend on the doping configurations, type, and level. Doping configuration, doping level, and type differ in all heteroatom-doped graphenes due to various starting graphene material, heteroatom precursor/source, doping temperature, and reaction time used in the synthesis method. Various synthesis approaches have been developed for heteroatom doping. Regardless of the enormous progress made so far, it is still a challenge to control the heteroatom doping. The research based on graphene will continue to grow vigorously due to the wide application of heteroatom-doped graphenes and new opportunities. It is foreseen that, sooner rather than later, after some improvement, such heteroatom-doped graphenes could be utilized for the necessities of society. In the near future, the heteroatom-doped graphene could play a major role in solving the energy-related issues in various solar cells, apart from applying it as CE in DSSCs.

ACKNOWLEDGEMENTS

The authors would like to thank the National Research Foundation (NRF), University of KwaZulu-Natal (UKZN), and UKZN Nanotechnology Platform for financial support. Also, the authors are grateful to Prof Bice Martincigh and Prof Tony Ford for proofreading the manuscript.

FUNDING INFORMATION

National Research Foundation (Grant numbers—101357 and 103979)

ORCID

Vincent O. Nyamori https://orcid.org/0000-0002-8995-4593

REFERENCES

1. Solangi K, Islam M, Saidur R, Rahim N, Fayaz H. A review on global solar energy policy. *Renew Sust Energy Rev.* 2011;15:2149-2163.
2. Haehnlein S, Bayer P, Blum P. International legal status of the use of shallow geothermal energy. *Renew Sust Energy Rev.* 2010;14:2611-2625.
3. Lund JW, Freeston DH, Boyd TL. Direct utilization of geothermal energy 2010 worldwide review. *Geothermics.* 2011;40:159-180.
4. Posten C, Schaub G. Microalgae and terrestrial biomass as source for fuels—a process view. *J Biotechnol.* 2009;142:64-69.
5. Azarpour A, Suhaimi S, Zahedi G, Bahadori A. A review on the drawbacks of renewable energy as a promising energy source of the future. *Arab J Sci Eng.* 2013;38:317-328.
6. Raheem A, Abbasi SA, Memon A, et al. Renewable energy deployment to combat energy crisis in Pakistan. *Energy Sustain Soc.* 2016;6:16.
7. Gokcol C, Dursun B, Alboyaci B, Sunan E. Importance of biomass energy as alternative to other sources in Turkey. *Energy Policy.* 2009;37:424-431.
8. Komerath N, Komerath P. Terrestrial micro renewable energy applications of space technology. *Phys Procedia.* 2011;20:255-269.
9. Okoro O, Madueme T. Solar energy: a necessary investment in a developing economy. *Int J Sustain Energy.* 2006;25:23-31.
10. Fuller MC, Portis SC, Kammen DM. Toward a low-carbon economy: municipal financing for energy efficiency and solar power. *Environ Sci Policy Sustain Dev.* 2009;51:22-33.
11. Sangani K. Power solar—the sun in your pocket. *Eng Technol.* 2007;2:36-38.
12. Sharma S, Jain KK, Sharma A. Solar cells: In research and applications—a review. *Mater Sci Appl.* 2015;6:1145.
13. Zhang S, Pan X, Jiao H, et al. 335-W world-record p-type monocrystalline module with 20.6% efficient PERC solar cells. *IEEE J Photovolt.* 2016;6:145-152.
14. Chopra K, Paulson P, Dutta V. Thin-film solar cells: an overview. *Prog Photovolt Res Appl.* 2004;12:69-92.

15. Major J, Treharne R, Phillips L, Durose K. A low-cost non-toxic post-growth activation step for CdTe solar cells. *Nature.* 2014;511:334.
16. Khosroabadi S, Keshmiri S, Marjani S. Design of a high efficiency CdS/CdTe solar cell with optimized step doping, film thickness, and carrier lifetime of the absorption layer. *J Eur Opt Soc Rapid Publ.* 2014;9:14052.
17. Kaur M, Singh H. A review: comparison of silicon solar cells and thin film solar cells. *Int J Core Eng Manag.* 2016;3:15-23.
18. Guo Q, Ford GM, Yang W-C, et al. Fabrication of 7.2% efficient CZTSSe solar cells using CZTS nanocrystals. *J Am Chem Soc.* 2010;132:17384-17386.
19. Li G, Zhu R, Yang Y. Polymer solar cells. *Nature Photonics.* 2012;6:153.
20. Liu Y, Zhao J, Li Z, et al. Aggregation and morphology control enables multiple cases of high-efficiency polymer solar cells. *Nat commun.* 2014;5:5293.
21. Chen JD, Cui C, Li YQ, et al. Single-junction polymer solar cells exceeding 10% power conversion efficiency. *Adv Mater.* 2015;27:1035-1041.
22. Guter W, Schöne J, Philipps SP, et al. Current-matched triple-junction solar cell reaching 41.1% conversion efficiency under concentrated sunlight. *Appl Phys Lett.* 2009;94:223504.
23. Hosoya M, Oooka H, Nakao H, et al. Module development for polymer solar cells, Abstract O-PV-6-2. *Grand Renew Energy Conf.* 2014;21-37.
24. Wei L, Wang P, Yang Y, et al. Enhanced performance of the dye-sensitized solar cells by the introduction of graphene oxide into the TiO_2 photoanode. *Inorg Chem Front.* 2018;5:54-62.
25. Freitag M, Teuscher J, Saygili Y, et al. Dye-sensitized solar cells for efficient power generation under ambient lighting. *Nature Photonics.* 2017;11:372.
26. Suhaimi S, Shahimin MM, Alahmed Z, Chyský J, Reshak A. Materials for enhanced dye-sensitized solar cell performance: electrochemical application. *Int J Electrochem Sci.* 2015;10:2859-2871.
27. Bagher AM, Vahid MMA, Mohsen M. Types of solar cells and application. *Am J Opt Photonics.* 2015;3:94-113.
28. Chiba Y, Islam A, Watanabe Y, Komiya R, Koide N, Han L. Dye-sensitized solar cells with conversion efficiency of 11.1%. *Jpn J Appl Phys.* 2006;45:L638.
29. Mishra A, Fischer MK, Bäuerle P. Metal-free organic dyes for dye-sensitized solar cells: from structure:property relationships to design rules. *Angew Chem Int Ed.* 2009;48:2474-2499.
30. Wu J, Lan Z, Lin J, et al. Electrolytes in dye-sensitized solar cells. *Chem Rev.* 2015;115:2136-2173.
31. Wu M, Ma T. Recent progress of counter electrode catalysts in dye-sensitized solar cells. *J Phys Chem C.* 2014;118:16727-16742.
32. Wei D. Dye sensitized solar cells. *Int J Mol Sci.* 2010;11:1103-1113.
33. Hagfeldt A, Boschloo G, Sun L, Kloo L, Pettersson H. Dye-sensitized solar cells. *Chem Rev.* 2010;110:6595-6663.
34. Uthirakumar P. *Solar Cells—Dye-Sensitized Devices: Fabrication of ZnO Based Dye-Sensitized Solar Cells.* India: IntechOpen; 2011.
35. Durrant JR, Haque SA, Palomares E. Photochemical energy conversion: from molecular dyads to solar cells. *Chem Commun (Camb).* 2006;3279-3289.
36. Lenzmann F, Krueger J, Burnside S, et al. Surface photovoltage spectroscopy of dye-sensitized solar cells with TiO_2, Nb_2O_5, and $SrTiO_3$ nanocrystalline photoanodes: indication for electron injection from higher excited dye states. *J Phys Chem B.* 2001;105:6347-6352.
37. Kanai Y, Grossman CJ. Insights on interfacial charge transfer across P_3HT/fullerene photovoltaic heterojunction from ab initio calculations. *Nano Lett.* 2007;7:1967-1972.
38. Stinchcombe J, Pbnicaud A, Bhyrappa P, Boyd DWP, Reed AC. Buckminsterfulleride (1-) salts: synthesis, EPR, and the Jahn-Teller distortion of C_{60}. *J Am Chem Soc.* 1993;115:5212-5217.
39. Dai L. Functionalization of graphene for efficient energy conversion and storage. *Acc Chem Res.* 2013;46:31-42.
40. Hu C, Liu D, Xiao Y, Dai L. Functionalization of graphene materials by heteroatom-doping for energy conversion and storage. *Prog Nat Sci-Mater.* 2018;28:121-132.
41. Ju MJ, Jeon I-Y, Kim HM, et al. Edge-selenated graphene nanoplatelets as durable metal-free catalysts for iodine reduction reaction in dye-sensitized solar cells. *Sci Adv.* 2016;56:1-8.
42. Hauch A, Georg A. Diffusion in the electrolyte and charge-transfer reaction at the platinum electrode in dye-sensitized solar cells. *Electrochim Acta.* 2001;46:3457-3466.
43. Huang Z, Liu X, Li K, et al. Application of carbon materials as counter electrodes of dye-sensitized solar cells. *Electrochem Commun.* 2007;9:596-598.
44. Nam JG, Park YJ, Kim BS, Lee JS. Enhancement of the efficiency of dye-sensitized solar cell by utilizing carbon nanotube counter electrode. *Scr Mater.* 2010;62:148-150.
45. Scalia A, Bella F, Lamberti A, et al. A flexible and portable powerpack by solid-state supercapacitor and dye-sensitized solar cell integration. *J Power Sources.* 2017;359:311-321.
46. Huo J, Wu J, Zheng M, Tu Y, Lan Z. Hydrothermal synthesis of CoMoO4/Co9S8 hybrid nanotubes based on counter electrodes for highly efficient dye-sensitized solar cells. *RSC Adv.* 2015;5:83029-83035.
47. Dao V-D, Choi H-S. Pt nanourchins as efficient and robust counter electrode materials for dye-sensitized solar cells. *ACS Appl Mater Interfaces.* 2015;8:1004-1010.
48. Xiao Y, Han G. Efficient hydrothermal-processed platinum–nickel bimetallic nano-catalysts for use in dye-sensitized solar cells. *J Power Sources.* 2015;294:8-15.
49. Moharana M, Mallik A. Nickel electrocrystallization in different electrolytes: an in-process and post synthesis analysis. *Electrochim Acta.* 2013;98:1-10.
50. Zhong C, Hu WB, Cheng YF. On the essential role of current density in electrocatalytic activity of the electrodeposited platinum for oxidation of ammonia. *J Power Sources.* 2011;196:8064-8072.

51. Tang Z, Wu J, Zheng M, Huo J, Lan Z. A microporous platinum counter electrode used in dye-sensitized solar cells. *Nano Energy.* 2013;2:622-627.
52. Wu M-S, Chen C-Y, Chen Y-R, Shih H-C. Synthesis of bimodal mesoporous carbon with embedded nickel nanoparticles through pyrolysis of nickel-organic framework as a counter-electrode catalyst for dye-sensitized solar cells. *Electrochim Acta.* 2016;215:50-56.
53. Hsu Y-C, Chen G-L, Lee R-H. Graphene oxide sheet-polyaniline nanocomposite prepared through in-situ polymerization/deposition method for counter electrode of dye-sensitized solar cell. *J Polym Res.* 2014;21:440.
54. Anothumakkool B, Agrawal I, Bhange SN, et al. Pt-and TCO-free flexible cathode for DSSC from highly conducting and flexible PEDOT paper prepared *via in situ* interfacial polymerization. *ACS Appl Mater Interfaces.* 2015;8:553-562.
55. Moraes RS, Saito E, Leite DMG, Massi M, da Silva Sobrinho AS. Optical, electrical and electrochemical evaluation of sputtered platinum counter electrodes for dye-sensitized solar cells. *Appl Surf Sci.* 2016;364:229-234.
56. Cheng X-Y, Zhou Z-J, Hou Z-L, Zhou W-H, Wu S-X. High performance dye-sensitized solar cell using $CuInGaSe_2$ as counter electrode prepared by sputtering. *Sci Adv Mater.* 2013;5:1193-1198.
57. Kang JS, Park M-A, Kim J-Y, et al. Reactively sputtered nickel nitride as electrocatalytic counter electrode for dye- and quantum dot-sensitized solar cells. *Sci Rep.* 2015;5:10450.
58. Wu J, Lan Z, Lin J, et al. Counter electrodes in dye-sensitized solar cells. *Chem Sov Rev.* 2017;46:5975-6023.
59. Gong F, Wang H, Xu X, Zhou G, Wang Z-S. In situ growth of $Co_{0.85}Se$ and $Ni_{0.85}Se$ on conductive substrates as high-performance counter electrodes for dye-sensitized solar cells. *J Am Chem Soc.* 2012;134:10953-10958.
60. Cha SI, Koo BK, Seo S, Lee DY. Pt-free transparent counter electrodes for dye-sensitized solar cells prepared from carbon nanotube micro-balls. *J Mater Chem.* 2010;20:659-662.
61. Lei B, Li G, Gao X. Morphology dependence of molybdenum disulfide transparent counter electrode in dye-sensitized solar cells. *J Mater Chem A.* 2014;2:3919-3925.
62. Yeh M-H, Lin L-Y, Lee C-P, et al. A composite catalytic film of PEDOT: PSS/TiN–NPs on a flexible counter-electrode substrate for a dye-sensitized solar cell. *J Mater Chem.* 2011;21:19021-19029.
63. Fang X, Ma T, Akiyama M, Guan G, Tsunematsu S, Abe E. Flexible counter electrodes based on metal sheet and polymer film for dye-sensitized solar cells. *Thin Solid Films.* 2005;472:242-245.
64. Ikegami M, Miyoshi K, Miyasaka T, et al. Platinum/titanium bilayer deposited on polymer film as efficient counter electrodes for plastic dye-sensitized solar cells. *Appl Phys Lett.* 2007;90:153122.
65. Li G, Song J, Pan G, Gao X. Highly Pt-like electrocatalytic activity of transition metal nitrides for dye-sensitized solar cells. *Energy Environ Sci.* 2011;4:1680-1683.
66. Yue G, Wu J, Xiao Y, et al. Platinum/graphene hybrid film as a counter electrode for dye-sensitized solar cells. *Electrochim Acta.* 2013;92:64-70.
67. Lee Y-L, Chen C-L, Chong L-W, Chen C-H, Liu Y-F, Chi C-F. A platinum counter electrode with high electrochemical activity and high transparency for dye-sensitized solar cells. *Electrochem Commun.* 2010;12:1662-1665.
68. Lee WJ, Ramasamy E, Lee DY, Song JS. Performance variation of carbon counter electrode based dye-sensitized solar cell. *Sol Energy Mater Sol Cells.* 2008;92:814-818.
69. Kim S-S, Nah Y-C, Noh Y-Y, Jo J, Kim D-Y. Electrodeposited Pt for cost-efficient and flexible dye-sensitized solar cells. *Electrochim Acta.* 2006;51:3814-3819.
70. Fang X, Ma T, Guan G, Akiyama M, Kida T, Abe E. Effect of the thickness of the Pt film coated on a counter electrode on the performance of a dye-sensitized solar cell. *J Electroanal Chem.* 2004;570:257-263.
71. Calogero G, Calandra P, Irrera A, Sinopoli A, Citro I, Di Marco G. A new type of transparent and low cost counter-electrode based on platinum nanoparticles for dye-sensitized solar cells. *Energ Environ Sci.* 2011;4:1838-1844.
72. Yen M-Y, Teng C-C, Hsiao M-C, et al. Platinum nanoparticles/graphene composite catalyst as a novel composite counter electrode for high performance dye-sensitized solar cells. *J Mater Chem.* 2011;21:12880-12888.
73. Huang K-C, Wang Y-C, Dong R-X, et al. A high performance dye-sensitized solar cell with a novel nanocomposite film of PtNP/MWCNT on the counter electrode. *J Mater Chem.* 2010;20:4067-4073.
74. Zhang B, Wang D, Hou Y, et al. Facet-dependent catalytic activity of platinum nanocrystals for triiodide reduction in dye-sensitized solar cells. *Sci Rep.* 2013;3:1836.
75. Olsen E, Hagen G, Eric Lindquist S. Dissolution of platinum in methoxy propionitrile containing LiI/I_2. *Sol Energy Mater Sol Cells.* 2000;63:267-273.
76. Deng X, Wu Y, Dai J, Kang D, Zhang D. Electronic structure tuning and band gap opening of graphene by hole/electron codoping. *Phys Lett.* 2011;375:3890-3894.
77. Ci L, Song L, Jin C, et al. Atomic layers of hybridized boron nitride and graphene domains. *Nat Mater.* 2010;9:430-435.
78. Xin X, He M, Han W, Jung J, Lin Z. Low-cost copper zinc tin sulfide counter electrodes for high-efficiency dye-sensitized solar cells. *Angew Chem Int Ed.* 2011;50:11739-11742.
79. Yasuo C, Ashraful I, Yuki W, Ryoichi K, Naoki K, Liyuan H. Dye-sensitized solar cells with conversion efficiency of 11.1%. *Jpn J Appl Phys.* 2006;45:L638.
80. Hsieh C-T, Yang B-H, Lin J-Y. One-and two-dimensional carbon nanomaterials as counter electrodes for dye-sensitized solar cells. *Carbon.* 2011;49:3092-3097.
81. Suzuki K, Yamaguchi M, Kumagai M, Yanagida S. Application of carbon nanotubes to counter electrodes of dye-sensitized solar cells. *Chem Lett.* 2002;32:28-29.
82. Hu X, Huang K, Fang D, Liu S. Enhanced performances of dye-sensitized solar cells based on graphite–TiO_2 composites. *Mater Sci Eng B.* 2011;176:431-435.

83. Roy-Mayhew JD, Aksay IA. Graphene materials and their use in dye-sensitized solar cells. *Chem Rev.* 2014;114:6323-6348.
84. Aqel A, Abou El-Nour K, Ammar R, Al-Warthan A. Carbon nanotubes, science and technology part (I) structure, synthesis and characterisation. *Arab J Chem.* 2012;5:1-23.
85. Chung D. Review graphite. *J Mater Sci.* 2002;37:1475-1489.
86. Allen MJ, Tung VC, Kaner RB. Honeycomb carbon: a review of graphene. *Chem Rev.* 2010;110:132-145.
87. Novoselov KS, Geim AK, Morozov SV, et al. Electric field effect in atomically thin carbon films. *Science.* 2004;306:666-669.
88. Miao X, Tongay S, Petterson MK, et al. High efficiency graphene solar cells by chemical doping. *Nano Lett.* 2012;12:2745-2750.
89. Castro EV, Novoselov K, Morozov S, et al. Biased bilayer graphene: semiconductor with a gap tunable by the electric field effect. *Phys Rev Lett.* 2007;99:216802.
90. Meyer JC, Geim AK, Katsnelson MI, Novoselov KS, Booth TJ, Roth S. The structure of suspended graphene sheets. *Nature.* 2007;446:60-63.
91. Boehm HP, Setton R, Stumpp E. Nomenclature and terminology of graphite intercalation compounds (IUPAC Recommendations 1994). *Pure Appl Chem.* 1994;66:1893-1901.
92. Zhu W, Perebeinos V, Freitag M, Avouris P. Carrier scattering, mobilities, and electrostatic potential in monolayer, bilayer, and trilayer graphene. *Phys Rev B.* 2009;80:235402.
93. Lu M-N, Chang C-Y, Wei T-C, Lin J-Y. Recent development of graphene-based cathode materials for dye-sensitized solar cells. *J Nanomater.* 2016;2016.
94. Koshino M, Ando T. Orbital diamagnetism in multilayer graphenes: systematic study with the effective mass approximation. *Phys Rev B.* 2007;76:085425.
95. Ohta T, Bostwick A, Seyller T, Horn K, Rotenberg E. Controlling the electronic structure of bilayer graphene. *Science.* 2006;313:951-954.
96. Zhang Y, Tang T-T, Girit C, et al. Direct observation of a widely tunable bandgap in bilayer graphene. *Nature.* 2009;459:820-823.
97. Tong X, Wei Q, Zhan X, Zhang G, Sun S. The new graphene family materials: synthesis and applications in oxygen reduction reaction. *Catalysts.* 2016;7:1.
98. Shen J, Zhu Y, Yang X, Li C. Graphene quantum dots: emergent nanolights for bioimaging, sensors, catalysis and photovoltaic devices. *Chem Commun.* 2012;48:3686-3699.
99. Guo S, Dong S. Graphene nanosheet: synthesis, molecular engineering, thin film, hybrids, and energy and analytical applications. *Chem Soc Rev.* 2011;40:2644-2672.
100. Yan X, Cui X, Li L-s. Synthesis of large, stable colloidal graphene quantum dots with tunable size. *J Am Chem Soc.* 2010;132:5944-5945.
101. Duan J, Chen S, Jaroniec M, Qiao SZ. Heteroatom-doped graphene-based materials for energy-relevant electrocatalytic processes. *ACS Catal.* 2015;5:5207-5234.
102. Ritter KA, Lyding JW. The influence of edge structure on the electronic properties of graphene quantum dots and nanoribbons. *Nat Mater.* 2009;8:235-242.
103. Morozov S, Novoselov K, Katsnelson M, et al. Giant intrinsic carrier mobilities in graphene and its bilayer. *Phy Rev Lett.* 2008;100:016602.
104. Avouris P. Graphene: electronic and photonic properties and devices. *Nano Lett.* 2010;10:4285-4294.
105. Xie G, Zhang K, Guo B, Liu Q, Fang L, Gong JR. Graphene-based materials for hydrogen generation from light-driven water splitting. *Adv Mater.* 2013;25:3820-3839.
106. Berger C, Song Z, Li X, et al. Electronic confinement and coherence in patterned epitaxial graphene. *Science.* 2006;312:1191-1196.
107. Cooper DR, D'Anjou B, Ghattamaneni N, et al. Experimental review of graphene. *ISRN Condens Matter Phys.* 2012;2012:1-56.
108. Neto AC, Guinea F, Peres NM, Novoselov KS, Geim AK. The electronic properties of graphene. *Rev Mod Phys.* 2009;81:109.
109. Liu J, Tang J, Gooding JJ. Strategies for chemical modification of graphene and applications of chemically modified graphene. *J Mater Chem.* 2012;22:12435-12452.
110. Niyogi S, Bekyarova E, Itkis ME, et al. Spectroscopy of covalently functionalized graphene. *Nano Lett.* 2010;10:4061-4066.
111. Chang Y-C, Chiang W-H. *Advances in Nanomaterials*. Germany: Springer Science and Business Media; 2016:103-133.
112. Wen Y, Huang C, Wang L, Hulicova-Jurcakova D. Heteroatom-doped graphene for electrochemical energy storage. *Sci Bulletin.* 2014;59:2102-2121.
113. Liang J, Huang Y, Zhang L, et al. Molecular-level dispersion of graphene into poly (vinyl alcohol) and effective reinforcement of their nanocomposites. *Adv Funct Mater.* 2009;19:2297-2302.
114. Rafiee MA, Rafiee J, Wang Z, Song H, Yu Z, Koratkar N. Enhanced mechanical properties of nanocomposites at low graphene content. *ACS Nano.* 2009;3:3884-3890.
115. Liu J, Yang W, Zareie HM, Gooding JJ, Davis TP. pH-detachable polymer brushes formed using titanium-diol coordination chemistry and living radical polymerization (RAFT). *Macromolecules.* 2009;42:2931-2939.
116. Sutter P, Sadowski JT, Sutter EA. Chemistry under cover: tuning metal-graphene interaction by reactive intercalation. *J Am Chem Soc.* 2010;132:8175-8179.
117. Sreeprasad T, Maliyekkal MS, Deepti K, Chaudhari K, Xavier PL, Pradeep T. Transparent, luminescent, antibacterial and patternable film forming composites of graphene oxide/reduced graphene oxide. *ACS Appl Mater Interfaces.* 2011;3:2643-2654.
118. Han TH, Lee WJ, Lee DH, Kim JE, Choi EY, Kim SO. Peptide/graphene hybrid assembly into core/shell nanowires. *Adv Mater.* 2010;22:2060-2064.
119. Li X, Wang H, Robinson JT, Sanchez H, Diankov G, Dai H. Simultaneous nitrogen doping and reduction of graphene oxide. *J Am Chem Soc.* 2009;131:15939-15944.
120. Yang X, Zhang X, Liu Z, Ma Y, Huang Y, Chen Y. High-efficiency loading and controlled release of doxorubicin

hydrochloride on graphene oxide. *J Phys Chem C.* 2008;112:17554-17558.

121. Raghu AV, Lee YR, Jeong HM, Shin CM. Preparation and physical properties of waterborne polyurethane/functionalized graphene sheet nanocomposites. *Macromol Chem Phys.* 2008;209:2487-2493.
122. Steenackers M, Gigler AM, Zhang N, et al. Polymer brushes on graphene. *J Am Chem Soc.* 2011;133:10490-10498.
123. Kim J, Cote LJ, Kim F, Huang J. Visualizing graphene based sheets by fluorescence quenching microscopy. *J Am Chem Soc.* 2009;132:260-267.
124. Yan L, Zheng YB, Zhao F, et al. Chemistry and physics of a single atomic layer: strategies and challenges for functionalization of graphene and graphene-based materials. *Chem Soc Rev.* 2012;41:97-114.
125. Scheuermann GM, Rumi L, Steurer P, Bannwarth W, Mülhaupt R. Palladium nanoparticles on graphite oxide and its functionalized graphene derivatives as highly active catalysts for the Suzuki-Miyaura coupling reaction. *J Am Chem Soc.* 2009;131:8262-8270.
126. McAllister MJ, Li J-L, Adamson DH, et al. Single sheet functionalized graphene by oxidation and thermal expansion of graphite. *Chem Mater.* 2007;19:4396-4404.
127. Yang S, Zhi L, Tang K, Feng X, Maier J, Müllen K. Efficient synthesis of heteroatom (N or S)-doped graphene based on ultrathin graphene oxide-porous silica sheets for oxygen reduction reactions. *Adv Funct Mater.* 2012;22:3634-3640.
128. Wang X, Sun G, Routh P, Kim D-H, Huang W, Chen P. Heteroatom-doped graphene materials: syntheses, properties and applications. *Chem Soc Rev.* 2014;43:7067-7098.
129. Gao W, Alemany LB, Ci L, Ajayan PM. New insights into the structure and reduction of graphite oxide. *Nat Chem.* 2009;1:403-408.
130. Shin HJ, Kim KK, Benayad A, et al. Efficient reduction of graphite oxide by sodium borohydride and its effect on electrical conductance. *Adv Funct Mater.* 2009;19:1987-1992.
131. Szabó T, Berkesi O, Forgó P, et al. Evolution of surface functional groups in a series of progressively oxidized graphite oxides. *Chem Mater.* 2006;18:2740-2749.
132. Balog R, Jørgensen B, Nilsson L, et al. Bandgap opening in graphene induced by patterned hydrogen adsorption. *Nat Mater.* 2010;9:315-319.
133. Wu Z-S, Ren W, Xu L, Li F, Cheng H-M. Doped graphene sheets as anode materials with superhigh rate and large capacity for lithium ion batteries. *ACS Nano.* 2011;5:5463-5471.
134. Blake P, Brimicombe PD, Nair RR, et al. Graphene-based liquid crystal device. *Nano Lett.* 2008;8:1704-1708.
135. Samuels AJ, Carey JD. Molecular doping and band-gap opening of bilayer graphene. *ACS Nano.* 2013;7:2790-2799.
136. Wehling T, Novoselov K, Morozov S, et al. Molecular doping of graphene. *Nano Lett.* 2008;8:173-177.
137. Chen W, Qi D, Gao X, Wee ATS. Surface transfer doping of semiconductors. *Prog Surf Sci.* 2009;84:279-321.
138. Chen W, Chen S, Qi DC, Gao XY, Wee ATS. Surface transfer p-type doping of epitaxial graphene. *J Am Chem Soc.* 2007;129:10418-10422.
139. Schedin F, Geim A, Morozov S, et al. Detection of individual gas molecules adsorbed on graphene. *Nat Mater.* 2007;6:652.
140. Ristein J. Surface transfer doping of semiconductors. *Science.* 2006;313:1057.
141. Leenaerts O, Partoens B, Peeters F. Adsorption of H_2O, NH_3, CO, NO_2, and NO on graphene: a first-principles study. *Phys Rev B.* 2008;77:125416.
142. Pontes RB, Fazzio A, Dalpian GM. Barrier-free substitutional doping of graphene sheets with boron atoms: ab initio calculations. *Phys Rev B.* 2009;79:033412.
143. Wang H, Wang Q, Cheng Y, et al. Doping monolayer graphene with single atom substitutions. *Nano Lett.* 2012;12:141-144.
144. Joucken F, Tison Y, Lagoute J, et al. Localized state and charge transfer in nitrogen-doped graphene. *Phys Rev B.* 2012;85:161408.
145. Jeon I-Y, Shin Y-R, Sohn G-J, et al. Edge-carboxylated graphene nanosheets *via* ball milling. *Proc Natl Acad Sci USA.* 2012;109:5588-5593.
146. Chang C-K, Kataria S, Kuo C-C, et al. Band gap engineering of chemical vapor deposited graphene by in situ BN doping. *ACS Nano.* 2013;7:1333-1341.
147. Lu X, Wu J, Lin T, et al. Low-temperature rapid synthesis of high-quality pristine or boron-doped graphenevia Wurtz-type reductive coupling reaction. *J Mater Chem.* 2011;21:10685-10689.
148. Deng D, Pan X, Yu L, et al. Toward N-doped graphene *via* solvothermal synthesis. *Chem Mater.* 2011;23:1188-1193.
149. Wu P, Cai Z, Gao Y, Zhang H, Cai C. Enhancing the electrochemical reduction of hydrogen peroxide based on nitrogen-doped graphene for measurement of its releasing process from living cells. *Chem Commun.* 2011;47:11327-11329.
150. Wu P, Qian Y, Du P, Zhang H, Cai C. Facile synthesis of nitrogen-doped graphene for measuring the releasing process of hydrogen peroxide from living cells. *J Mater Chem.* 2012;22:6402-6412.
151. Jeong HM, Lee JW, Shin WH, et al. Nitrogen-doped graphene for high-performance ultracapacitors and the importance of nitrogen-doped sites at basal planes. *Nano Lett.* 2011;11:2472-2477.
152. Li N, Wang Z, Zhao K, Shi Z, Gu Z, Xu S. Large scale synthesis of N-doped multi-layered graphene sheets by simple arc-discharge method. *Carbon.* 2010;48:255-259.
153. Duplock EJ, Scheffler M, Lindan PJD. Hallmark of perfect graphene. *Phys Rev Lett.* 2004;92:225502.
154. Cheng JL, Salazar C, Sipe JE. Optical properties of functionalized graphene. *Phys Rev B.* 2013;88:045438.
155. Kannan AG, Zhao J, Jo S-G, Kang YS, Kim D-W. Nitrogen and sulfur co-doped graphene counter electrodes with synergistically enhanced performance for dyesensitized solar cells. *J Mater Chem A.* 2018;2:12232-12239.
156. Dreyer DR, Park S, Bielawski CW, Ruoff RS. The chemistry of graphene oxide. *Chem Soc Rev.* 2010;39:228-240.

157. Garg R, Dutta NK, Choudhury NR. Work function engineering of graphene. *Nanomaterials.* 2014;4:267-300.

158. Lee DW, Seo JW. sp^2/sp^3 carbon ratio in graphite oxide with different preparation times. *J Phys Chem C.* 2011;115:2705-2708.

159. Compton OC, Nguyen ST. Graphene oxide, highly reduced graphene oxide, and graphene: versatile building blocks for carbon-based materials. *Small.* 2010;6:711-723.

160. Zhong YL, Tian Z, Simon GP, Li D. Scalable production of graphene via wet chemistry: progress and challenges. *Mater Today.* 2015;18:73-78.

161. Brodie BC. On the atomic weight of graphite. *Phil Trans R Soc Lond.* 1859;149:249-259.

162. Staudenmaier L. Process for the preparation of graphitic acid. *Eur J Inorg Chem.* 1898;31:1481-1487.

163. Hofmann U, König E. Studies on graphite oxide. *Z Anorg Allg Chem.* 1937;234:311-336.

164. Hummers WS Jr, Offeman RE. Preparation of graphitic oxide. *J Am Chem Soc.* 1958;80:1339-1339.

165. Zaaba NI, Foo KL, Hashim U, Tan SJ, Liu W-W, Voon CH. Synthesis of graphene oxide using modified hummers method: solvent influence. *Procedia Eng.* 2017;184:469-477.

166. Yu H, Zhang B, Bulin C, Li R, Xing R. High-efficient synthesis of graphene oxide based on improved Hummers method. *Sci Rep.* 2016;6:36143.

167. Marcano DC, Kosynkin DV, Berlin JM, et al. Improved synthesis of graphene oxide. *ACS Nano.* 2010;4:4806-4814.

168. Chen D, Feng H, Li J. Graphene oxide: preparation, functionalization, and electrochemical applications. *Chem Rev.* 2012;112:6027-6053.

169. Xu J, Dong G, Jin C, Huang M, Guan L. Sulfur and nitrogen co-doped, few-layered graphene oxide as a highly efficient electrocatalyst for the oxygen-reduction reaction. *ChemSusChem.* 2013;6:493-499.

170. Ambrosi A, Chua CK, Bonanni A, Pumera M. Lithium aluminum hydride as reducing agent for chemically reduced graphene oxides. *Chem Mater.* 2012;24:2292-2298.

171. Moon IK, Lee J, Ruoff RS, Lee H. Reduced graphene oxide by chemical graphitization. *Nat commun.* 2010;1:73.

172. Tegou E, Pseiropoulos G, Filippidou MK, Chatzandroulis S. Low-temperature thermal reduction of graphene oxide films in ambient atmosphere: infra-red spectroscopic studies and gas sensing applications. *Microelectron Eng.* 2016;159:146-150.

173. Garino N, Sacco A, Castellino M, et al. Microwave-assisted synthesis of reduced graphene oxide/SnO2 nanocomposite for oxygen reduction reaction in microbial fuel cells. *ACS Appl Mater Interfaces.* 2016;8:4633-4643.

174. Matsumoto Y, Koinuma M, Kim SY, et al. Simple photoreduction of graphene oxide nanosheet under mild conditions. *ACS Appl Mater Interfaces.* 2010;2:3461-3466.

175. Ng YH, Iwase A, Kudo A, Amal R. Reducing graphene oxide on a visible-light $BiVO_4$ photocatalyst for an enhanced photoelectrochemical water splitting. *J Phys Chem Lett.* 2010;1:2607-2612.

176. Pham VH, Cuong TV, Hur SH, et al. Chemical functionalization of graphene sheets by solvothermal reduction of a graphene oxide suspension in N-methyl-2-pyrrolidone. *J Mater Chem.* 2011;21:3371-3377.

177. Nethravathi C, Rajamathi M. Chemically modified graphene sheets produced by the solvothermal reduction of colloidal dispersions of graphite oxide. *Carbon.* 2008;46:1994-1998.

178. Dubin S, Gilje S, Wang K, et al. A one-step, solvothermal reduction method for producing reduced graphene oxide dispersions in organic solvents. *ACS Nano.* 2010;4:3845-3852.

179. Long D, Li W, Ling L, Miyawaki J, Mochida I, Yoon S-H. Preparation of nitrogen-doped graphene sheets by a combined chemical and hydrothermal reduction of graphene oxide. *Langmuir.* 2010;26:16096-16102.

180. Mathkar A, Tozier D, Cox P, et al. Controlled, stepwise reduction and band gap manipulation of graphene oxide. *J Phys Chem Lett.* 2012;3:986-991.

181. Hanifah MFR, Jaafar J, Aziz M, Ismail A, Othman M, Rahman MA. Effects of reduction time on the structural, electrical and thermal properties of synthesized reduced graphene oxide nanosheets. *Bull Mater Sci.* 2015;38:1569-1576.

182. Pei S, Cheng H-M. The reduction of graphene oxide. *Carbon.* 2012;50:3210-3228.

183. Eda G, Chhowalla M. Chemically derived graphene oxide: towards large-area thin-film electronics and optoelectronics. *Adv Mater.* 2010;22:2392-2415.

184. Maiti R, Midya A, Narayana C, Ray S. Tunable optical properties of graphene oxide by tailoring the oxygen functionalities using infrared irradiation. *Nanotechnology.* 2014;25:495704.

185. Pham TA, Kim J, Kim JS, Jeong YT. Corrigendum to "One-step reduction of graphene oxide with l-glutathione". *Colloids Surf A Physicochem Eng Asp.* 2011;386:195.

186. Lei Z, Lu L, Zhao X. The electrocapacitive properties of graphene oxide reduced by urea. *Energy Environ Sci.* 2012;5:6391-6399.

187. Stankovich S, Dikin DA, Piner RD, et al. Synthesis of graphene-based nanosheets via chemical reduction of exfoliated graphite oxide. *Carbon.* 2007;45:1558-1565.

188. Zhang J, Yang H, Shen G, Cheng P, Zhang J, Guo S. Reduction of graphene oxide via L-ascorbic acid. *Chem Commun.* 2010;46:1112-1114.

189. Fan X, Peng W, Li Y, et al. Deoxygenation of exfoliated graphite oxide under alkaline conditions: a green route to graphene preparation. *Adv Mater.* 2008;20:4490-4493.

190. Li Z, Yao Y, Lin Z, Moon K-S, Lin W, Wong C. Ultrafast, dry microwave synthesis of graphene sheets. *J Mater Chem.* 2010;20:4781-4783.

191. Mei X, Ouyang J. Ultrasonication-assisted ultrafast reduction of graphene oxide by zinc powder at room temperature. *Carbon.* 2011;49:5389-5397.

192. Yeh M-H, Lin L-Y, Chang L-Y, et al. Dye-sensitized solar cells with reduced graphene oxide as the counter electrode prepared by a green photothermal reduction process. *ChemPhysChem.* 2014;15:1175-1181.

193. Cote LJ, Cruz-Silva R, Huang J. Flash reduction and patterning of graphite oxide and its polymer composite. *J Am Chem Soc.* 2009;131:11027-11032.

194. Chien CT, Li SS, Lai WJ, et al. Tunable photoluminescence from graphene oxide. *Angew Chem Int Ed.* 2012;51:6662-6666.

195. Wu P, Du P, Zhang H, Cai C. Microscopic effects of the bonding configuration of nitrogen-doped graphene on its reactivity toward hydrogen peroxide reduction reaction. *Phys Chem Chem Phys.* 2013;15:6920-6928.

196. Xing Z, Ju Z, Zhao Y, et al. One-pot hydrothermal synthesis of nitrogen-doped graphene as high-performance anode materials for lithium ion batteries. *Sci Rep.* 2016;6:26146.

197. Zhang C, Fu L, Liu N, Liu M, Wang Y, Liu Z. Synthesis of nitrogen-doped graphene using embedded carbon and nitrogen sources. *Adv Mater.* 2011;23:1020-1024.

198. Shao Y, Zhang S, Engelhard MH, et al. Nitrogen-doped graphene and its electrochemical applications. *J Mater Chem.* 2010;20:7491-7496.

199. Biddinger EJ, von Deak D, Ozkan US. Nitrogen-containing carbon nanostructures as oxygen-reduction catalysts. *Top Catal.* 2009;52:1566-1574.

200. Ewels C, Glerup M. Nitrogen doping in carbon nanotubes. *J Nanosci Nanotechnol.* 2005;5:1345-1363.

201. Kundu S, Nagaiah TC, Xia W, et al. Electrocatalytic activity and stability of nitrogen-containing carbon nanotubes in the oxygen reduction reaction. *J Phys Chem C.* 2009;113:14302-14310.

202. Groves M, Chan A, Malardier-Jugroot C, Jugroot M. Improving platinum catalyst binding energy to graphene through nitrogen doping. *Chem Phys Lett.* 2009;481:214-219.

203. Lherbier A, Blase X, Niquet Y-M, Triozon F, Roche S. Charge transport in chemically doped 2D graphene. *Phys Rev Lett.* 2008;101:036808.

204. Wu M, Cao C, Jiang JZ. Light non-metallic atom (B, N, O and F)-doped graphene: a first-principles study. *Nanotechnology.* 2010;21:505202.

205. Wei D, Liu Y, Wang Y, Zhang H, Huang L, Yu G. Synthesis of N-doped graphene by chemical vapor deposition and its electrical properties. *Nano Lett.* 2009;9:1752-1758.

206. Yanilmaz A, Tomak A, Akbali B, et al. Nitrogen doping for facile and effective modification of graphene surfaces. *RSC Advances.* 2017;7:28383-28392.

207. Du M, Sun J, Chang J, Yang F, Shi L, Gao L. Synthesis of nitrogen-doped reduced graphene oxide directly from nitrogen-doped graphene oxide as a high-performance lithium ion battery anode. *RSC Adv.* 2014;4:42412-42417.

208. Lu Y-F, Lo S-T, Lin J-C, et al. Nitrogen-doped graphene sheets grown by chemical vapor deposition: synthesis and influence of nitrogen impurities on carrier transport. *ACS Nano.* 2013;7:6522-6532.

209. Shinde SM, Kano E, Kalita G, Takeguchi M, Hashimoto A, Tanemura M. Grain structures of nitrogen-doped graphene synthesized by solid source-based chemical vapor deposition. *Carbon.* 2016;96:448-453.

210. Capasso A, Dikonimos T, Sarto F, et al. Nitrogen-doped graphene films from chemical vapor deposition of pyridine: influence of process parameters on the electrical and optical properties. *Beilstein J Nanotechnol.* 2015;6:2028.

211. Dadkhah A, Faradonbeh M, Rashidi A, Tasharrofi S, Mansourkhani F. One step synthesis of nitrogen-doped graphene from naphthalene and urea by atmospheric chemical vapor deposition. *J Inorg Organomet Polym Mater.* 2018;28:1609-1615.

212. Bundaleska N, Henriques J, Abrashev M, et al. Large-scale synthesis of free-standing N-doped graphene using microwave plasma. *Sci Rep.* 2018;8:12595.

213. Kumar A, Voevodin A, Paul R, et al. Nitrogen-doped graphene by microwave plasma chemical vapor deposition. *Thin Solid Films.* 2013;528:269-273.

214. Shah SA, Cui L, Lin K, et al. Preparation of novel silicon/nitrogen-doped graphene composite nanosheets by DC arc discharge. *RSC Adv.* 2015;5:29230-29237.

215. Li D, Duan X, Sun H, et al. Facile synthesis of nitrogen-doped graphene via low-temperature pyrolysis: the effects of precursors and annealing ambience on metal-free catalytic oxidation. *Carbon.* 2017;115:649-658.

216. Jiang M-H, Cai D, Tan N. Nitrogen-doped graphene sheets prepared from different graphene-based precursors as high capacity anode materials for lithium-ion batteries. *Int J Electrochem Sci.* 2017;12:7154-7165.

217. Rybin M, Pereaslavtsev A, Vasilieva T, et al. Efficient nitrogen doping of graphene by plasma treatment 2015.

218. Guo B, Liu Q, Chen E, Zhu H, Fang L, Gong JR. Controllable N-doping of graphene. *Nano Lett.* 2010;10:4975-4980.

219. Geng D, Chen Y, Chen Y, et al. High oxygen-reduction activity and durability of nitrogen-doped graphene. *Energy Environ Sci.* 2011;4:760-764.

220. Wang X, Li X, Zhang L, et al. N-doping of graphene through electrothermal reactions with ammonia. *Science.* 2009;324:768-771.

221. Wang H, Maiyalagan T, Wang X. Review on recent progress in nitrogen-doped graphene: synthesis, characterization, and its potential applications. *ACS Catal.* 2012;2:781-794.

222. Sheng Z-H, Shao L, Chen J-J, Bao W-J, Wang F-B, Xia X-H. Catalyst-free synthesis of nitrogen-doped graphene via thermal annealing graphite oxide with melamine and its excellent electrocatalysis. *ACS Nano.* 2011;5:4350-4358.

223. Śliwak A, Grzyb B, Díez N, Gryglewicz G. Nitrogen-doped reduced graphene oxide as electrode material for high rate supercapacitors. *Appl Surf Sc.* 2017;399:265-271.

224. Chen Y, Xie B, Ren Y, et al. Designed nitrogen doping of few-layer graphene functionalized by selective oxygenic groups. *Nanoscale Res Lett.* 2014;9:646.

225. Alexander M, Roumen V, Koen S, et al. Synthesis of few-layer graphene *via* microwave plasma-enhanced chemical vapour deposition. *Nanotechnology.* 2008;19:305604.

226. Janowska I, Chizari K, Ersen O, et al. Microwave synthesis of large few-layer graphene sheets in aqueous solution of ammonia. *Nano Res.* 2010;3:126-137.

227. Hutchison J, Kiselev N, Krinichnaya E, et al. Double-walled carbon nanotubes fabricated by a hydrogen arc discharge method. *Carbon.* 2001;39:761-770.

228. Panchakarla L, Subrahmanyam K, Saha S, et al. Synthesis, structure, and properties of boron-and nitrogen-doped graphene. *Adv Mater.* 2009;21:4726-4730.

229. Lee HC, Liu W-W, Chai S-P, et al. Synthesis of single-layer graphene: a review of recent development. *Procedia Chem.* 2016;19:916-921.

230. Liu H, Liu Y, Zhu D. Chemical doping of graphene. *J Mater Chem.* 2011;21:3335-3345.

231. Nandamuri G, Roumimov S, Solanki R. Chemical vapor deposition of graphene films. *Nanotechnology.* 2010;21:145604.

232. Wang Z, Li P, Chen Y, et al. Synthesis of nitrogen-doped graphene by chemical vapour deposition using melamine as the sole solid source of carbon and nitrogen. *J Mater Chem C.* 2014;2:7396-7401.

233. Reddy ALM, Srivastava A, Gowda SR, Gullapalli H, Dubey M, Ajayan PM. Synthesis of nitrogen-doped graphene films for lithium battery application. *ACS Nano.* 2010;4:6337-6342.

234. Jin Z, Yao J, Kittrell C, Tour JM. Large-scale growth and characterizations of nitrogen-doped monolayer graphene sheets. *ACS Nano.* 2011;5:4112-4117.

235. Van Nang L, Van Duy N, Hoa ND, Van Hieu N. Nitrogen-doped graphene synthesized from a single liquid precursor for a field effect transistor. *J Electron Mater.* 2016;45:839-845.

236. Imamura G, Saiki K. Synthesis of nitrogen-doped graphene on Pt (111) by chemical vapor deposition. *J Phys Chem C.* 2011;115:10000-10005.

237. Ci L, Song L, Jin C, et al. Atomic layers of hybridized boron nitride and graphene domains. *Nat Mater.* 2010;9:430-435.

238. Qu L, Liu Y, Baek J-B, Dai L. Nitrogen-doped graphene as efficient metal-free electrocatalyst for oxygen reduction in fuel cells. *ACS Nano.* 2010;4:1321-1326.

239. Cho YJ, Kim HS, Baik SY, et al. Selective nitrogen-doping structure of nanosize graphitic layers. *J Phys Chem C.* 2011;115:3737-3744.

240. Luo Z, Lim S, Tian Z, et al. Pyridinic N doped graphene: synthesis, electronic structure, and electrocatalytic property. *J Mater Chem.* 2011;21:8038-8044.

241. Zhang C, Lin W, Zhao Z, et al. CVD synthesis of nitrogen-doped graphene using urea. *Sci China Phys Mech.* 2015;58:107801.

242. Bayram E, Yilmaz G, Mukerjee S. A solution-based procedure for synthesis of nitrogen doped graphene as an efficient electrocatalyst for oxygen reduction reactions in acidic and alkaline electrolytes. *Appl Catal B.* 2016;192:26-34.

243. Lv W-X, Zhang R, Xia T-L, Bi H-M, Shi K-Y. Influence of NH_3 flow rate on pyridine-like N content and NO electrocatalytic oxidation of N-doped multiwalled carbon nanotubes. *J Nanoparticle Res.* 2011;13:2351-2360.

244. Mukherjee S, Kaloni T. Electronic properties of boron-and nitrogen-doped graphene: a first principles study. *J Nanoparticle Res.* 2012;14:1059.

245. Agnoli S, Favaro M. Doping graphene with boron: a review of synthesis methods, physicochemical characterization, and emerging applications. *J Mater Chem A.* 2016;4:5002-5025.

246. Rani P, Jindal V. Designing band gap of graphene by B and N dopant atoms. *RSC Adv.* 2013;3:802-812.

247. Miwa RH, Martins TB, Fazzio A. Hydrogen adsorption on boron doped graphene: an ab initio study. *Nanotechnology.* 2008;19:155708.

248. Faccio R, Fernández-Werner L, Pardo H, Goyenola C, Ventura ON, Mombrú ÁW. Electronic and structural distortions in graphene induced by carbon vacancies and boron doping. *J Phys Chem C.* 2010;114:18961-18971.

249. Tang Y-B, Yin L-C, Yang Y, et al. Tunable band gaps and p-type transport properties of boron-doped graphenes by controllable ion doping using reactive microwave plasma. *ACS Nano.* 2012;6:1970-1978.

250. Zhao L, Levendorf M, Goncher S, et al. Local atomic and electronic structure of boron chemical doping in monolayer graphene. *Nano Lett.* 2013;13:4659-4665.

251. Kim YA, Fujisawa K, Muramatsu H, et al. Raman spectroscopy of boron-doped single-layer graphene. *ACS Nano.* 2012;6:6293-6300.

252. Endo M, Hayashi T, Hong S-H, Enoki T, Dresselhaus MS. Scanning tunneling microscope study of boron-doped highly oriented pyrolytic graphite. *J Appl Phys.* 2001;90:5670-5674.

253. Borowiec J, Zhang J. Hydrothermal synthesis of boron-doped graphene for electrochemical sensing of guanine. *J Electrochem Soc.* 2015;162:B332-B336.

254. Tian Z, Xu C, Li J, et al. A facile preparation route for highly conductive borate cross-linked reduced graphene oxide paper. *New J Chem.* 2015;39:6907-6913.

255. Zhao L, Levendorf M, Goncher S, et al. Local atomic and electronic structure of boron chemical doping in monolayer graphene. *Nano Lett.* 2013;13:4659-4665.

256. Ovezmyradov M, Magedov IV, Frolova LV, et al. Chemical vapor deposition of phosphorous-and boron-doped graphene using phenyl-containing molecules. *J Nanosci Nanotechnol.* 2015;15:4883-4886.

257. Tour JM. Top-down versus bottom-up fabrication of graphene-based electronics. *J Chem Mater.* 2014;26:163-171.

258. Panchakarla L, Subrahmanyam K, Saha S, et al. Synthesis, structure and properties of boron and nitrogen doped graphene. *Adv Mater.* 2009;21:4726-4730.

259. Li S, Wang Z, Jiang H, et al. Plasma-induced highly efficient synthesis of boron doped reduced graphene oxide for supercapacitors. *Chem Commun.* 2016;52:10988-10991.

260. Sheng Z-H, Gao H-L, Bao W-J, Wang F-B, Xia X-H. Synthesis of boron doped graphene for oxygen reduction reaction in fuel cells. *J Mater Chem.* 2012;22:390-395.

261. Fang H, Yu C, Ma T, Qiu J. Boron-doped graphene as a high-efficiency counter electrode for dye-sensitized solar cells. *Chem Commun.* 2014;50:3328-3330.

262. Telychko M, Mutombo P, Ondráček M, et al. Achieving high-quality single-atom nitrogen doping of graphene/SiC(0001) by

ion implantation and subsequent thermal stabilization. *ACS Nano.* 2014;8:7318-7324.

263. Usachov DY, Fedorov AV, Petukhov AE, et al. Epitaxial B-graphene: large-scale growth and atomic structure. *ACS Nano.* 2015;9:7314-7322.
264. Cattelan M, Agnoli S, Favaro M, et al. Microscopic view on a chemical vapor deposition route to boron-doped graphene nanostructures. *J Chem Mater.* 2013;25:1490-1495.
265. Wu T, Shen H, Sun L, Cheng B, Liu B, Shen J. Nitrogen and boron doped monolayer graphene by chemical vapor deposition using polystyrene, urea and boric acid. *New J Chem.* 2012;36:1385-1391.
266. Wang H, Zhou Y, Wu D, et al. Synthesis of boron-doped graphene monolayers using the sole solid feedstock by chemical vapor deposition. *Small.* 2013;9:1316-1320.
267. Yang Z, Yao Z, Li G, et al. Sulfur-doped graphene as an efficient metal-free cathode catalyst for oxygen reduction. *ACS Nano.* 2012;6:205-211.
268. Yang Z, Yao Z, Li G, et al. Sulfur-doped graphene as an efficient metal-free cathode catalyst for oxygen reduction. *ACS Nano.* 2011;6:205-211.
269. Denis PA. Band gap opening of monolayer and bilayer graphene doped with aluminium, silicon, phosphorus, and sulfur. *Chem Phys Lett.* 2010;492:251-257.
270. Denis PA, Faccio R, Mombru AW. Is It possible to dope single-walled carbon nanotubes and graphene with sulfur? *Chemphyschem.* 2009;10:715-722.
271. Hassani F, Tavakol H, Keshavarzipour F, Javaheri A. A simple synthesis of sulfur-doped graphene using sulfur powder by chemical vapor deposition. *RSC Adv.* 2016;6:27158-27163.
272. Xia Y, Zhu Y, Tang Y. Preparation of sulfur-doped microporous carbons for the storage of hydrogen and carbon dioxide. *Carbon.* 2012;50:5543-5553.
273. Poh HL, Šimek P, Sofer Z k, Pumera M. Sulfur-doped graphene via thermal exfoliation of graphite oxide in H_2S, SO_2, or CS_2 gas. *ACS Nano.* 2013;7:5262-5272.
274. Liang C, Wang Y, Li T. Synthesis of sulfur-doped p-type graphene by annealing with hydrogen sulfide. *Carbon.* 2015;82:506-512.
275. Bautista-Flores C, Arellano-Peraza J, Sato-Berrú R, Camps E, Mendoza D. Sulfur and few-layer graphene interaction under thermal treatments. *Chem Phys Lett.* 2016;665:121-126.
276. Kiciński W, Szala M, Bystrzejewski M. Sulfur-doped porous carbons: synthesis and applications. *Carbon.* 2014;68:1-32.
277. Gao H, Liu Z, Song L, et al. Synthesis of S-doped graphene by liquid precursor. *Nanotechnology.* 2012;23:275605.
278. Liu Y, Ma Y, Jin Y, Chen G, Zhang X. Microwave-assisted solvothermal synthesis of sulfur-doped graphene for electrochemical sensing. *J Electroanal Chem.* 2015;739:172-177.
279. Liu ZW, Peng F, Wang HJ, Yu H, Zheng WX, Yang J. Phosphorus-doped graphite layers with high electrocatalytic activity for the O_2 reduction in an alkaline medium. *Angew Chem.* 2011;123:3315-3319.
280. Yang D-S, Bhattacharjya D, Song MY, Yu J-S. Highly efficient metal-free phosphorus-doped platelet ordered mesoporous carbon for electrocatalytic oxygen reduction. *Carbon.* 2014;67:736-743.
281. Cruz-Silva E, Lopez-Urias F, Munoz-Sandoval E, et al. Electronic transport and mechanical properties of phosphorus- and phosphorus-nitrogen-doped carbon nanotubes. *ACS Nano.* 2009;3:1913-1921.
282. Denis PA. Band gap opening of monolayer and bilayer graphene doped with aluminium, silicon, phosphorus, and sulfur. *Chemical Physics Letters.* 2010;492:251-257.
283. Wang H-m, Wang H-x, Chen Y, et al. Phosphorus-doped graphene and (8, 0) carbon nanotube: structural, electronic, magnetic properties, and chemical reactivity. *Appl Surf Sci.* 2013;273:302-309.
284. Some S, Kim J, Lee K, et al. Highly air-stable phosphorus-doped n-type graphene field-effect transistors. *Adv Mater.* 2012;24:5481-5486.
285. Sun Z, Yan Z, Yao J, Beitler E, Zhu Y, Tour JM. Growth of graphene from solid carbon sources. *Nature.* 2010;468:549-552.
286. Yen W-C, Medina H, Huang J-S, et al. Direct synthesis of graphene with tunable work function on insulators *via in situ* boron doping by nickel-assisted growth. *J Phys Chem C.* 2014;118:25089-25096.
287. Zhang C, Mahmood N, Yin H, Liu F, Hou Y. Synthesis of phosphorus-doped graphene and its multifunctional applications for oxygen reduction reaction and lithium ion batteries. *Adv Mater.* 2013;25:4932-4937.
288. Wen Y, Wang B, Huang C, Wang L, Hulicova-Jurcakova D. Synthesis of phosphorus-doped graphene and its wide potential window in aqueous supercapacitors. *Chem Eur J.* 2015;21:80-85.
289. Shin D-W, Kim TS, Yoo J-B. Phosphorus doped graphene by inductively coupled plasma and triphenylphosphine treatments. *Mater Res Bull.* 2016;82:71-75.
290. Li R, Wei Z, Gou X, Xu W. Phosphorus-doped graphene nanosheets as efficient metal-free oxygen reduction electrocatalysts. *RSC Adv.* 2013;3:9978-9984.
291. Denis PA. Concentration dependence of the band gaps of phosphorus and sulfur doped graphene. *Comput Mater Sci.* 2013;67:203-206.
292. Latorre-Sánchez M, Primo A, García H. P-doped graphene obtained by pyrolysis of modified alginate as a photocatalyst for hydrogen generation from water–methanol mixtures. *Angew Chem Int Ed.* 2013;52:11813-11816.
293. Kakaei K, Balavandi A. Synthesis of halogen-doped reduced graphene oxide nanosheets as highly efficient metal-free electrocatalyst for oxygen reduction reaction. *J Colloid Interface Sci.* 2016;463:46-54.
294. Yang K, Li Y, Tan X, Peng R, Liu Z. Behavior and toxicity of graphene and its functionalized derivatives in biological systems. *Small.* 2013;9:1492-1503.
295. Kalyani R, Gurunathan K. Intercalated network of graphene oxide (GO)–CuO–polythiophene (PTh) hybrid nanocomposite for photocatalytic applications. *J Mater Sci Mater Electron.* 2016;27:10634-10641.

296. Ciobotaru IC, Polosan S, Ciobotaru CC. Organometallic compounds for photovoltaic applications. *Inorganica Chim Acta.* 2018;483:448-453.

297. Zbořil R, Karlický F, Bourlinos AB, et al. Graphene fluoride: a stable stoichiometric graphene derivative and its chemical conversion to graphene. *Small.* 2010;6:2885-2891.

298. Shen B, Chen J, Yan X, Xue Q. Synthesis of fluorine-doped multi-layered graphene sheets by arc-discharge. *RSC Adv.* 2012;2:6761-6764.

299. Wu J, Xie L, Li Y, et al. Controlled chlorine plasma reaction for non-invasive graphene doping. *J Am Chem Soc.* 2011;133:19668-19671.

300. Yaya A, Ewels C, Suarez-Martinez I, et al. Bromination of graphene and graphite. *Phys Rev B.* 2011;83:045411.

301. Jeon I-Y, Choi H-J, Choi M, et al. Facile, scalable synthesis of edge-halogenated graphene nanoplatelets as efficient metal-free eletrocatalysts for oxygen reduction reaction. *Sci Rep.* 2013;3:1810.

302. Bouša D, Pumera M, Sedmidubský D, et al. Fine tuning of graphene properties by modification with aryl halogens. *Nanoscale.* 2016;8:1493-1502.

303. Sharma R, Khan S, Goyal V, Sharma V, Sharma KS. Investigation on effect of boron and nitrogen substitution on electronic structure of graphene. *Chem Flat Mater.* 2017;1:20-33.

304. Muchharla B, Pathak A, Liu Z, et al. Tunable electronics in large-area atomic layers of boron–nitrogen–carbon. *Nano Lett.* 2013;13:3476-3481.

305. Ma L, Hart AHC, Ozden S, Vajtai R, Ajayan PM. Spiers memorial lecture advances of carbon nanomaterials. *Faraday Discussions.* 2014;173:9-46.

306. Wu ZS, Winter A, Chen L, et al. Three-dimensional nitrogen and boron co-doped graphene for high-performance all-solid-state supercapacitors. *Adv Mater.* 2012;24:5130-5135.

307. Bepete G, Voiry D, Chhowalla M, Chiguvare Z, Coville NJ. Incorporation of small BN domains in graphene during CVD using methane, boric acid and nitrogen gas. *Nanoscale.* 2013;5:6552-6557.

308. Choi CH, Chung MW, Kwon HC, Park SH, Woo SI. B, N-and P, N-doped graphene as highly active catalysts for oxygen reduction reactions in acidic media. *J Mater Chem A.* 2013;1:3694-3699.

309. Thomas S, Deepak T, Anjusree G, Arun T, Nair SV, Nair AS. A review on counter electrode materials in dye-sensitized solar cells. *J Mater Chem A.* 2014;2:4474-4490.

310. Xue Y, Wu B, Liu H, Tan J, Hu W, Liu Y. Direct synthesis of phosphorus and nitrogen co-doped monolayer graphene with air-stable n-type characteristics. *Phys Chem Chem Phys.* 2014;16:20392-20397.

311. Wang Z-L, Xu D, Wang H-G, Wu Z, Zhang X-B. In situ fabrication of porous graphene electrodes for high-performance energy storage. *ACS Nano.* 2013;7:2422-2430.

312. Wang T, Wang L-X, Wu D-L, Xia W, Jia D-Z. Interaction between nitrogen and sulfur in co-doped graphene and synergetic effect in supercapacitor. *Sci Rep.* 2015;5:9591.

313. Yang Z, Qian K, Lv J, et al. Encapsulation of Fe_3O_4 nanoparticles into N, S co-doped graphene sheets with greatly enhanced electrochemical performance. *Sci Rep.* 2016;6:27957.

314. Xing T, Zheng Y, Li LH, et al. Observation of active sites for oxygen reduction reaction on nitrogen-doped multilayer graphene. *ACS Nano.* 2014;8:6856-6862.

315. Li J, Zhang Y, Zhang X, et al. S, N dual-doped graphene-like carbon nanosheets as efficient oxygen reduction reaction electrocatalysts. *ACS Appl Mater Interfaces.* 2017;9:398-405.

316. Roy-Mayhew JD, Bozym DJ, Punckt C, Aksay IA. Functionalized graphene as a catalytic counter electrode in dye-sensitized solar cells. *ACS Nano.* 2010;4:6203-6211.

317. Boschloo G, Hagfeldt A. Characteristics of the iodide/triiodide redox mediator in dye-sensitized solar cells. *Acc Chem Res.* 2009;42:1819-1826.

318. Hardin BE, Snaith HJ, McGehee MD. The renaissance of dye-sensitized solar cells. *Nature Photonics.* 2012;6:162.

319. Dao V-D, Larina LL, Suh H, Hong K, Lee J-K, Choi H-S. Optimum strategy for designing a graphene-based counter electrode for dye-sensitized solar cells. *Carbon.* 2014;77:980-992.

320. Kavan L, Yum JH, Grätzel M. Optically transparent cathode for dye-sensitized solar cells based on graphene nanoplatelets. *ACS Nano.* 2010;5:165-172.

321. Devarepally KK. Low cost fabrication of graphene oxide films as efficient counter electrode for dye-sensitized solar cells (DSSC). *Meeting Abstracts*. 2016;**MA2016-01**:775.

322. Zheng H, Neo CY, Mei X, Qiu J, Ouyang J. Reduced graphene oxide films fabricated by gel coating and their application as platinum-free counter electrodes of highly efficient iodide/triiodide dye-sensitized solar cells. *J Mater Chem.* 2012;22:14465-14474.

323. Jang H-S, Yun J-M, Kim D-Y, Park D-W, Na S-I, Kim S-S. Moderately reduced graphene oxide as transparent counter electrodes for dye-sensitized solar cells. *Electrochim Acta.* 2012;81:301-307.

324. Xu X, Huang D, Cao K, Wang M, Zakeeruddin SM, Grätzel M. Electrochemically reduced graphene oxide multilayer films as efficient counter electrode for dye-sensitized solar cells. *Sci Rep.* 2013;3:1489.

325. Nagavolu C, Susmitha K, Raghavender M, et al. Pt-free spray coated reduced graphene oxide counter electrodes for dye sensitized solar cells. *Solar Energy.* 2016;137:143-147.

326. Jang H-S, Yun J-M, Kim D-Y, Na S-I, Kim S-S. Transparent graphene oxide–Pt composite counter electrode fabricated by pulse current electrodeposition-for dye-sensitized solar cells. *Surf Coat Technol.* 2014;242:8-13.

327. Sarker S, Lee K-S, Seo HW, Jin Y-K, Kim DM. Reduced graphene oxide for Pt-free counter electrodes of dye-sensitized solar cells. *Solar Energy.* 2017;158:42-48.

328. Zhang M, Dai L. Carbon nanomaterials as metal-free catalysts in next generation fuel cells. *Nano Energy.* 2012;1:514-517.

329. Xue Y, Liu J, Chen H, et al. Nitrogen-doped graphene foams as metal-free counter electrodes in high-performance dye-sensitized solar cells. *Angew Chem Int Ed.* 2012;51:12124-12127.

330. Wang G, Fang Y, Lin Y, Xing W, Zhuo S. Nitrogen-doped graphene as transparent counter electrode for efficient dye-sensitized solar cells. *Mater Res Bull.* 2012;47:4252-4256.

331. Hou S, Cai X, Wu H, et al. Nitrogen-doped graphene for dye-sensitized solar cells and the role of nitrogen states in triiodide reduction. *Energy & Environmental Science.* 2013;6:3356-3362.

332. Yen M-Y, Hsieh C-K, Teng C-C, et al. Metal-free, nitrogen-doped graphene used as a novel catalyst for dye-sensitized solar cell counter electrodes. *RSC Adv.* 2012;2:2725-2728.

333. Ju MJ, Kim JC, Choi H-J, et al. N-doped graphene nanoplatelets as superior metal-free counter electrodes for organic dye-sensitized solar cells. *ACS Nano.* 2013;7:5243-5250.

334. Ju MJ, Jeon I-Y, Kim JC, et al. Graphene nanoplatelets doped with nitrogen at its edges as metal-free cathodes for organic dye-sensitized solar cells. *Adv Mater.* 2014;26:3055-3062.

335. Lin C-A, Lee C-P, Ho S-T, et al. Nitrogen-doped graphene/platinum counter electrodes for dye-sensitized solar cells. *ACS Photonics.* 2014;1:1264-1269.

336. Xue Y, Baek JM, Chen H, Qu J, Dai L. N-doped graphene nanoribbons as efficient metal-free counter electrodes for disulfide/thiolate redox mediated DSSCs. *Nanoscale.* 2015;7:7078-7083.

337. Kim S-B, Park J-Y, Kim C-S, et al. Effects of graphene in dye-sensitized solar cells based on nitrogen-doped TiO_2 composite. *J Phys Chem C.* 2015;119:16552-16559.

338. Balamurugan J, Thanh TD, Kim NH, Lee JH. Nitrogen-doped graphene nanosheets with FeN core–shell nanoparticles as high-performance counter electrode materials for dye-sensitized solar cells. *Adv Mater Interfaces.* 2016;3:1500348.

339. Yang W, Xu X, Hou L, et al. Insight into the topological defects and dopants in metal-free holey graphene for triiodide reduction in dye-sensitized solar cells. *J Mater Chem A.* 2017;5:5952-5960.

340. Lin C-A, Lee C-P, Ho S-T, et al. Nitrogen-doped graphene/platinum counter electrodes for dye-sensitized solar cells. *ACS Photonics.* 2014;1:1264-1269.

341. Jung S-M, Choi IT, Lim K, et al. B-doped graphene as an electrochemically superior metal-free cathode material as compared to Pt over a Co (II)/Co (III) electrolyte for dye-sensitized solar cell. *Chem Mater.* 2014;26:3586-3591.

342. Ambrosi A, Chua CK, Bonanni A, Pumera M. Electrochemistry of graphene and related materials. *Chem Rev.* 2014;114:7150-7188.

343. Wang L, Sofer Z, Šimek P, Tomandl I, Pumera M. Boron-doped graphene: Scalable and tunable p-type carrier concentration doping. *J Phys Chem C.* 2013;117:23251-23257.

344. Luo Q, Hao F, Wang S, et al. Highly efficient metal-free sulfur-doped and nitrogen and sulfur dual-doped reduced graphene oxide counter electrodes for dye-sensitized solar cells. *J Phys Chem C.* 2014;118:17010-17018.

345. Meng X, Yu C, Song X, et al. Rational design and fabrication of sulfur-doped porous graphene with enhanced performance as a counter electrode in dye-sensitized solar cells. *J Mater Chem A.* 2017;5:2280-2287.

346. Mustafa MN, Shafie S, Zainal Z, Sulaiman Y. A novel poly (3, 4-ethylenedioxythiophene)-graphene oxide/titanium dioxide composites counter electrode for dye-sensitized solar cell. *J Nanomater.* 2017;2017.

347. Kaukonen M, Krasheninnikov AV, Kauppinen E, Nieminen RM. Doped graphene as a material for oxygen reduction reaction in hydrogen fuel cells: a computational study. *ACS Catal.* 2013;3:159-165.

348. Karthika P, Rajalakshmi N, Dhathathreyan K. Phosphorus-doped exfoliated graphene for supercapacitor electrodes. *J Nanosci Nanotechnol.* 2013;13:1746-1751.

349. Wang Z, Li P, Chen Y, et al. Phosphorus-doped reduced graphene oxide as an electrocatalyst counter electrode in dye-sensitized solar cells. *J Power Sources.* 2014;263:246-251.

350. Ahn H-J, Kim I-H, Yoon J-C, Kim S-I, Jang J-H. p-Doped three-dimensional graphene nano-networks superior to platinum as a counter electrode for dye-sensitized solar cells. *Chem Commun.* 2014;50:2412-2415.

351. Xu X, Yang W, Chen B, et al. Phosphorus-doped porous graphene nanosheet as metal-free electrocatalyst for triiodide reduction reaction in dye-sensitized solar cell. *Appl Surf Sci.* 2017;405:308-315.

352. Jeon I-Y, Kim HM, Choi IT, et al. High-performance dye-sensitized solar cells using edge-halogenated graphene nanoplatelets as counter electrodes. *Nano Energy.* 2015;13:336-345.

353. Yu D, Nagelli E, Du F, Dai L. Metal-free carbon nanomaterials become more active than metal catalysts and last longer. *J Phys Chem Lett.* 2010;1:2165-2173.

354. Das S, Sudhagar P, Verma V, et al. Amplifying charge-transfer characteristics of graphene for triiodide reduction in dye-sensitized solar cells. *Adv Funct Mater.* 2011;21:3729-3736.

355. Kannan AG, Zhao J, Jo SG, Kang YS, Kim D-W. Nitrogen and sulfur co-doped graphene counter electrodes with synergistically enhanced performance for dye-sensitized solar cells. *J Mater Chem A.* 2014;2:12232-12239.

356. Xu X, Yang W, Li Y, et al. Heteroatom-doped graphene-like carbon films prepared by chemical vapour deposition for bifacial dye-sensitized solar cells. *Chem Eng J.* 2015;267:289-296.

357. Yu Z, Bai Y, Wang Y, et al. One-step synthesis of three-dimensional nitrogen and sulfur co-doped graphene networks as low cost metal-free counter electrodes for dye-sensitized solar cells. *Chem Eng J.* 2017;311:302-309.

358. Wen Y, Rufford TE, Hulicova-Jurcakova D, Wang L. Nitrogen and phosphorous co-doped graphene monolith for supercapacitors. *Chem Sust Energy Mater.* 2016;9:513-520.

359. Yu D, Xue Y, Dai L. Vertically aligned carbon nanotube arrays co-doped with phosphorus and nitrogen as efficient metal-free electrocatalysts for oxygen reduction. *J Phys Chem Lett.* 2012;3:2863-2870.

360. Yu C, Liu Z, Meng X, Lu B, Cui D, Qiu J. Nitrogen and phosphorus dual-doped graphene as a metal-free high-efficiency electrocatalyst for triiodide reduction. *Nanoscale.* 2016;8:17458-17464.

361. Rani P, Dubey GS, Jindal VK. DFT study of optical properties of pure and doped graphene. *Physica E Low Dimens Sys Nanostruct.* 2014;62:28-35.

362. Chang DW, Choi H-J, Jeon I-Y, Baek J-B. Edge-selectively functionalized graphene nanoplatelets. *J Chem Soc Japan.* 2013;13:224-238.

363. Sivula K, Ball ZT, Watanabe N, Fréchet JMJ. Amphiphilic diblock copolymer compatibilizers and their effect on the morphology and performance of polythiophene:fullerene solar cells. *Adv Mater.* 2005;18:206-210.

364. O'Regan BC, Durrant JR. Kinetic and energetic paradigms for dye-sensitized solar cells: Moving from the ideal to the real. *Acc Chem Res.* 2009;42:1799-1808.

365. Gong J, Sumathy K, Qiao Q, Zhou Z. Review on dye-sensitized solar cells (DSSCs): advanced techniques and research trends. *Renew Sust Energy Rev.* 2017;68:234-246.

366. Bonaccorso F, Colombo L, Yu G, et al. Graphene, related two-dimensional crystals, and hybrid systems for energy conversion and storage. *Science.* 2015;347:1246501.

How to cite this article: Ngidi NPD, Ollengo MA, Nyamori VO. Heteroatom-doped graphene and its application as a counter electrode in dye-sensitized solar cells. *Int J Energy Res*. 2019;43:1702–1734. https://doi.org/10.1002/er.4326